NAZARBAYEV UNIVERSITY

Numerical Investigation of fault gouge material (FGM) Mechanical Behavior under the influence of pore pressure and loading conditions

Master of Science in Mining Engineering

Muhammad Yaqoob

Supervisor: Prof. Ali Mortazavi

School of Mining and Geosciences

Nazarbayev University

Date 29/04/2024

(a) Abstract

This research study presents a numerical analysis of the mechanical behavior of fault gouge materials (FGMs) using the finite element method (FEM) within the Abaqus computational analysis environment (CAE). The mechanical properties of fault zones are greatly influenced by fault gouge materials, which are fine-grained materials located inside fault planes. The mechanical behavior of FGM toward pore fluid pressure plays a crucial role in Carbon Capture and Storage (CCS) projects, which include the sequestration of CO_2 inside geological formations.

Previous research has shown the important role of fluid pore pressures in commencing fault displacement, which may either reduce or increase fault stability. Pore pressure fluctuation plays an important role in maintaining fault stability in completely saturated FGMs.

The purpose of this thesis is to analyze the behavior of fluid-saturated fine-grained materials (FGMs) under both normal and shear loading situations using Abaqus Finite Element Method (FEM) analysis. The study intends to address the limitations of currently available prediction models and contribute to the advancement of geomechanics knowledge in the context of FGM.

The comparative analysis evaluates the influence of pore pressure on the Fault Gouge Material (FGM) in both models. The FGM simulation findings indicate that the models without pore pressure exhibit slightly greater deformation compared to the models with pore pressure. However, while considering the elastic analysis, it is shown that the FGM demonstrates a greater degree of deformation when subjected to pore pressure under normal loading conditions.

(b) Declaration

I, **Muhammad Yaqoob,** hereby declare that this submission is my own work and to the best of my knowledge it contains no materials previously published or written by another person, or substantial proportions of material which have been accepted for the award of any other degree or diploma at Nazarbayev University or any other educational institution, except where due acknowledgement is made in the thesis.

Any contribution made to the research by others, with whom I have worked at NU or elsewhere is explicitly acknowledged in the thesis.

I also declare that the intellectual content of this thesis is the product of my own work, except to the extent that assistance from others in the project's design and conception or in style, presentation and linguistic expression is acknowledged.

Sign: 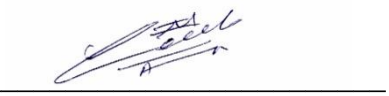

(c) Acknowledgement

I would like to express my profound gratitude to Prof. Ali Mortazavi, (SMG, Nazarbayev University) a technophile and a research minded personality, for his guidance and valuable suggestions. This work would not have been possible without his encouragement. I sincerely thank him for the time and patience he devoted for this work. Moreover, I thankful for the financial support provided by Chevron, through their grant program. This funding was significant in facilitating the research necessary to complete this thesis.

I also extend thanks to the all the faculty members of Mining department for their valuable suggestions.

Thank you

Table of Contents

List of Figures

List of Tables

1.Introduction

1.1 Background

It is very important to understand the behavior of fault gouge materials with pore fluid pressure conditions which is very important for the effective management and sealing structure of Carbon Capture Storage (CCS) projects. The influence of fault gouges on the seismic characteristics of fault zones is of the highest significance as they play a critical role in defining their strength and behavior. The mechanical properties of faults, including slip behavior, are greatly influenced by fault gouges, which consist of fine-grained materials along fault planes.

The correlation between fault gouges and pore fluid pressures is of significant interest due to its potential to induce both fault weakening and strengthening, hence impacting fault stability. The significance of pore fluid pressures within fault gouges have been highlighted by (Faulkner, et al. 2018) who demonstrated how change in pore pressure triggers the slip phenomena. (Hirakawa,et al 2016) conducted a study utilizing dynamic rupture models to illustrate the impact of inelastic compaction and dilatancy of fault gouge material on fault strength during seismic events. Their findings showed that these factors contribute to the dynamic weakening and strengthening of faults.

The study of fault gouge materials is relevant to Carbon Capture and Storage (CCS) efforts, particularly in the context of geomechanics and the integrity of storage reservoirs. In CCS, carbon dioxide (CO_2) captured from industrial sources is injected into geological formations for long-term storage to mitigate its release into the atmosphere. Understanding the behavior of fault gouges within these storage sites is crucial for ensuring the safety and effectiveness of CCS projects and mitigating potential risks associated with fluid flow through fault zones.

In fully saturated fault gouge, researchers have focused on the alteration of permeability and the variation of pore fluid pressure. The fault stability is greatly influenced by the mineralogical composition of fault gouges, particularly including clay-rich and non-clay fault gouge materials. Moreover, changes in fluid pore pressure can induce triggered seismicity, suggesting a potential link between fluid dynamics and the initiation of seismic events within fault zones (Scuderi, et al. 2016).

The above research works emphasize the complex nature of fault gouge materials behavior and its influence on fault slip mechanisms. Numerical modeling methods was used, acquire a good understanding of the fault gouge behavior under various stress load conditions.

1.2 FEM Model on Abaqus CAE

The finite element method (FEM) is a solid numerical approach used to solve a wide range of mechanical and computational issues related to the physical world. Abaqus CAE software by using the Finite Element Method (FEM), which is a powerful and flexible computational technique that offers a systematic framework for modeling and understanding the mechanical behavior of materials under different boundary and loading circumstances. Abaqus is a highly trusted and commonly used software package for finite element analysis (FEA) developed by Dassault Systèmes Simulia Corp (Update 2011), which allows engineers and researchers to model complex physical processes, offering a digital environment to analyze the performance of structures, materials, and systems under various conditions (Barbero 2023).

1.3 Problem statement

Fluids play a significant role in altering the characteristics of the slip behavior of the fault gouge materials. The following problems were identified to study the behavior of fault gouge materials under the influence of pore pressure.

- Effect of fluid presence
- Pore pressure effects
- Volume change characteristics

Therefore, it is important to develop a better understanding of fault gouge mechanical behavior to reduce the gap in current predictive models and research because of their economic and environmental significance for instance leakage problems in subsurface structures.

1.4 Objective

In this thesis work, our main objective is to understand the behavior of the fluid-saturated fault gouge materials (FGM) under normal and shear loading conditions to compare with the

unsaturated conditions of the gouge materials using Abaqus FEM analysis. Pore fluid pressure exert a considerable influence on modifying the slip behavior of gouge materials. Through this simulation on Abaqus, we can derive various outcomes related to pore fluid pressure within gouge-type materials:

This research aims to address this gap by conducting a comprehensive Abaqus Finite Element Method (FEM) analysis to provide a detailed study of fault gouge behavior under pore fluid pressure conditions.

- Assessment of how pore pressure influences the deformation rate of the gouge materials.
- Evaluating how pore pressure influences the shear behavior of the gouge materials.
- Analysis of how pore fluid pressure changes during shear response over displacement and time.

The initial steps set to meet the objectives in this thesis are outlined as follows:

- Literature review
- Numerical modeling on Abaqus
- Preliminary simulations
- Data analysis framework
- Model comparative analysis

1.5 The research significance to the industry

The future destination for capture of carbon dioxide (CO_2) is the deep and depleted oil and gas reservoirs (Bachu 2015). However, the main factor determining the long-term safety of CO_2 storage is the structural sealing capacity, which is crucial for ensuring the safe and secure storage of CO_2 over a long period (Phillips, et al. 2020).

So the sealing structure of fault zone, which is included a fault gouge, the crushed and pulverized fault rock in the fault and this fault gouge includes clay smear, and granular flow (Faulkner, et al. 2006). The Sealing capacity of Carbon Capture Storage (CCS) is mainly dependent on the different properties fault gouge material for instance pore pressure, permeability, coefficient of friction etc.

2. Literature Review

2.1 Introduction

A thorough review of fault gouge materials, including their mechanical behavior under stress, particularly about the influence of pore fluid pressure, is essential for understanding fault mechanics. Moreover, pore fluid pressure exert a considerable influence on modifying the slip behavior of gouge materials. This literature review provides a comprehensive analysis of numerous basic concepts of gouge materials, the important role of pore fluid pressure, and the utilization of numerical modeling in the field of geomechanics.

2.2 Fault Gouge Materials

To fault gouge materials refer to the crushed and pulverized rocks that accumulate along fault planes. These materials are often clay-rich or non-clay and have a mixture of soil rock mixture, which develops along different fault zones. This fragmented rock formed through the process of grinding and shearing of rock walls during fault movement. (Reches,et al. 2005) proposed and examined that fault gouge forms by the rock pulverization within the tip region of a fast propagating earthquake due to the intensity of stress and rates of strain in this zone. The accumulative wear product of slide between fault surfaces is most commonly referred to as a fault gouge. As it comes to the overall issue of fault mechanics, one of the most significant aspects is gaining an understanding of the role that gouges play in faulting and friction (Marone, et al. 1990).

The formation of a fine grain gouge in the center regions of fault zones is considered to control the frictional characteristics of faults and the resulting instability that leads to earthquakes (Ben-Zion, et al. 2003). Brittle fault-zones commonly show a characteristic reduction in grain size, resulting in the formation of breccia and gouge. There are several theories about the fine or grain size distribution of the gouge materials, ranging from few micro meter to cm. This is because the reduction of the grain size occurs during grain crushing, so it happens through the process of continuous grain crushing caused by increasing grain-contact stress (Sammis, et al. 1986).

2.3 Types of clay gouges

Fault gouge materials are mainly made up of granular substances, often containing clay or non-clay types. The primary categories classified into two types, as explained below.

a. Clay rich and non-clay rich fault gouge
b. Soil rock mixture fault gouge

a. Clay rich and non-Clay gouge materials

Normally, natural fault gouge consists of a high percentage of clay with sand having a different proportions by weight. Therefore, numerous research have attempted to define the transport properties of fault gouge by utilizing combinations of sand and clay. Kaolinite clay is frequently used as a representative clay in fault gouge examinations due to its basic chemistry and non-expansive properties. It has been shown via a multitude of studies that the clay-rich fault gouge material is the most common sort of gouge material (Faulkner et al. 2008), (Saffer et al. 2009)**.** It possesses a low permeability and clay has a significant impact on the properties of the gouge material.

For the above mention clay and sand rich fault gouge, the (Zheng, et al. 2021) conducted experiments on synthetic fault gouge made from sand and clay obtained from the Frio and Anahuac formations in the Gulf of Mexico. They analyzed the absolute permeability, breakthrough pressure, and relative permeability of the synthetic fault gouge, and the development of quantitative interactions for all of these mentioned properties based on the clay content in the gouge materials.

The research conducted by (Haines et al. 2013) offers significant knowledge regarding the organized formation and transformation of fabric elements in clay rich fault gouges materials, as a result of shear deformation. Fabric elements refers to the structural attributes that arise in due to external forces during the deformation processes. The features include mineral alignment, orientation, distribution, and qualities of fabric elements inside a material that is under deformation (Vannucchi, et al. 2003).These findings highlight the prevalent nature of fabric

evolution in materials rich in clay, providing insight into the fundamental mechanisms that control the deformation behavior and mechanical properties of fault gouges.

Gouge materials that are non-clay in nature exhibit diverse mechanical properties. These materials can comprise various rock types and may have different grain sizes, mineral compositions, and interlocking characteristics. Additionally, the presence of fractures or weaknesses within non-clay gouges can affect their mechanical behavior. Understanding the properties and behavior of non-clay gouge materials is crucial for assessing fault strength, frictional behavior, and slip propagation within fault zones (Morrow, et al. 1984). In deep mines and tunnels, it is common to find fault gouges with significant clay content, which have been observed at depths of up to 2 km (Brekke, et al 1973).

b. Soil-Rock Mixture for Fault Gouge Materials

It is possible to prepare fault gouge from a Soil Rock Mixture (SRM) which is also considered as a non-clay fault gouge material, but the process can be more challenging compared to preparing it from a homogenous sediment. SRMs often have a more complex composition and structure, with varying grain sizes and mineralogy, which can affect the mechanical properties of the resulting fault gouge. Soil Rock Mixture gouge materials for experimental lab testing purposes which was prepared artificially by (Tao,et al. 2022) by mixing of soil and rock consists of particles distributions of Soil < 5 mm, and rock 5 mm < 30 mm shown in Table 2.1

According to the author, the specification regarding the soil-rock threshold in SRM, as agreed upon by many scholars, and states that particles with a particle size less than 5 mm are considered fine soil, while those with a particle size greater than 5 mm are regarded as rock blocks.

Figure 2-1: SRM filling material (Tao, et al. 2022)

Table 2-1: Particle size distribution (Tao, et al. 2022)

	Rock							**Soil**
Particle size (mm)	>40	31.5-40	25-31.5	20-25	16-20	10-16	5-10	<5
Distributions (%)	6.15	1.88	2.15	11.33	3.5	11.76	9.86	53.37

The fault breccia and fault gouge mixture (SRM) that fills in faults zones contributes a crucial role in determining the deformation, permeability, and stability of the structures. This mixture typically exhibits a small deformation modulus, significant weathering, low strength, and high permeability (Zhang, et al. 2016)**.**

In soil rock mixture gouge materials, the rock particle content can have a large impact on its shear strength and properties of the materials. The large scale test, which includes the large direct shear test, the large triaxial test, and the in situ test, is the primary method that is utilized in all of the investigations that are conducted on the experimental mechanical properties of the soil-rock mixture fault gouge. A comprehensive investigation on the mechanical behavior of a soil-rock mixture in the Nuozhadu embankment dam was carried out by (Zhang, Xu et al. 2016). This investigation included two large-scale compaction test fields as well as a series of in situ direct

shear tests. (Fei 2016) carried out a series of triaxial tests on clay-steel bead and clay fine gravel combinations in order to gain an understanding of the influence that coarse particles have on the mechanical behavior of clay aggregate mixtures.(Wei, Xu et al. 2018) conducted a series of LDS (Large direct shear) experiments into investigate how varying water concentrations and grain size distributions affect the mechanical properties of the SRMs.

2.4 Mechanical and Hydrological parameters of the Fault gouge materials

The properties for the elastic model, to fallow the Hooke's law, which describes deformation in the elastic domain by establishing a relationship between stress and strain through an elasticity (or stiffness) matrix. If the substance is linear-elastic and isotropic, it is sufficient to consider only two material properties: Young's modulus and Poisson's ratio. The Young's modulus, also known as the modulus of elasticity. The Table 2.2 shows examples of elastic properties reported for the fault gouge material by different authors.

The Young's modulus of fault rocks, particularly intact rock, comes in within the 1-100 GPa range. Fault gauges, which commonly are used as representations of the fault core, exhibit Young's modulus values as low as 0.01 GPa (Treffeisen, et al. 2020).

Table 2-2: Average Input properties for Fault gouge materials

Property	**Average Value**	**Conditions**	**References**
Permeability (k)	10^{-10} to 10^{-22} m²	Highly dependent on clay content	Lockner (2009) Faulkner (2010)
Young's Modulus (E)	0.01 GPa	Varies with mineralogy and confining pressure	Treffeisen (2020)
Poisson's Ratio (ν)	0.2 to 0.3	Depends on composition and porosity	Faulkner et al. (2006)
Coefficient of Friction (μ)	0.3-0.45	lower in the presence of fluids and clay minerals	Byerlee (1978)
Pore Pressure	Variable		Zhang (2019)

The average values for the fault gouge materials in the fault zones, as shown in Table 2.2, are within the range of input parameters for the fault hydro-mechanical reservoir model in Finite Element Simulation suggested by (Treffeisen, et al. 2020). As illustrated in Table 3.3. From the fault gauges can have Young's modulus values as low as 0.01 GPa and permeability of 10^{-14} m^2.

Table 2-3: Mechanical and Hydraulic parameters used for the model (Treffeisen, et al. 2020)

Property	**Symbol**	**Fault Zone**	**Reservoir**	**Overburden**
Young's modulus (GPa)	E	0.1–10	30	30
Poissons' ratio	ν	0.1–0.25	0.23	0.23
Friction angle	φ	10–25	40	40
Cohesion (MPa)	c	0.01–5	20	20
Tensile strength (MPa)	T_0	5	20	20
Density (kg/m³)	ρ	2400	2400	2400
Permeability (m²)	k	10^{-14}	5^{-12}	10^{-17}

2.5 Permeability of the fault gouge materials

The permeability of fault gouge material can vary widely depending on various factors such as grain size, composition, compaction, and the presence of fluids. Fault gouge is composed of crushed and powdered rock material that fills the void space along a fault plane. To understand the alterations in permeability during the shearing deformation is essential for understanding the dynamic hydrological and mechanical phenomena that take place during earthquakes and seismic activity, both at shallow and deep levels within the Earth's crust (Rojstaczer, Wolf et al. 1995). The fault gouge mixture and fault gouge that present in faults zones contributes a crucial role in determining the deformation, permeability, and stability of the structures. This mixture typically exhibits a small deformation modulus, low strength, and high permeability (Zhang, Xu et al.

2016). The permeability (k) of fault gouge materials is highly variable and is heavily dependent on the clay content and the state of compaction within the fault gouge. It generally ranges between 10^-10 to 10^-22 m^2. (Morrow et al., 2017, Lockner et al., 2009**).**

The Sealing capacity of CCS storage is mainly dependent on different properties of fault gouge material such as permeability and breakthrough pressure. Breakthrough pressure is the minimum pressure which is required to displace or push one type of fluid out of small pores in a rock and replace it with another liquid in a interconnected pore systems. High breakthrough pressure fault rocks usually show to inhibit the fluid flow. The range of breakthrough pressures for synthetic clay rich gouge sample is 4 to 5 MPa for liquid CO2 and from 2.8 to 4.5 MPa for Supercritical CO2 (Makhnenko et al. 2017)**.**

To determine the permeability of fault gouge materials or fault rocks, various laboratory and field techniques are employed. Giger, et al. (2011) presents the development and validation of a novel fluid-sealed direct shear apparatus designed to investigate fault-related fluid flow under large displacement conditions. The study aims to improve the understanding of fluid behavior within geological faults during shearing events, which has implications for earthquake mechanics and reservoir engineering. The apparatus design is unique in its ability to maintain fluid confinement while allowing for substantial displacements during the shear testing process. This capability is crucial as it replicates real-world conditions where significant displacements can occur along faults during seismic events.(Giwelli, et al. 2016) used direct shearing experiments in a recent study to examine the hydro-mechanical changes that take place during faulting in carbonate rock. The study discovered that the dynamic transmissibility across the fault is permanently reduced after gouge material is produced in the fault zone's core. Additionally, the volume drops during shearing.

The permeability of fault gouge materials can decrease by several orders of magnitude when the clay content and effective stress are increased. According to literature, addition of clay leads to a slower reduction in permeability. The permeability of fault gouge can decrease by more than a 3 order of magnitude when the clay content increases up to 40 wt% (Faulkner et al. 2008).In case of effective stress (a 10 MPa increase in effective stress) the logarithm of fault gouge permeability decreases by order of 0.5 to 1 magnitude (Faulkner, et al. 2000, Giwelli et al. 2016)**.**

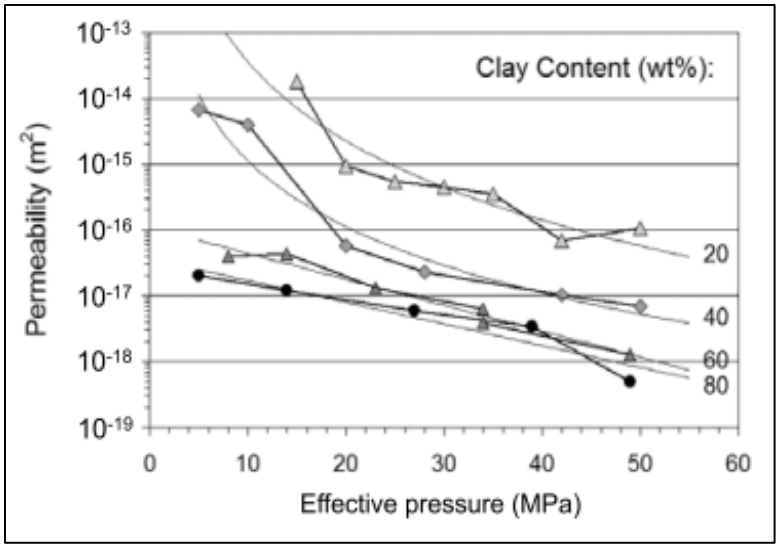

Figure 2-2: Permeability reduction in response to increase in effective pressure under hydrostatic loading (Faulkner et al. 2008)

In general, fault gouge material tends to have higher permeability compared to intact rock due to its fragmented nature. The crushed and pulverized grains create interconnected pathways that allow fluids, such as water or hydrocarbons, to flow more easily through the material. However, the actual permeability values can range from relatively high to very low, depending on the specific characteristics of the fault gouge. The study of fault zone behavior involves a particular focus on the fluid flow patterns and mechanical characteristics of gouge materials, including both clay-rich and non-clay compositions.

2.5.1 Role of pore pressure in fault gouge material behavior

Pore fluid pressure plays an important role in fault gouge mechanical behavior by weakening and reduce the effective normal stress which causes weakening of the shear stress acting on it thereby leading to sliding. A full understanding of fault mechanics and the factors contributing to seismic events and CO_2 leakage requires a thorough understanding of the role of pore pressure in fault gouge materials. The present review provides an in-depth review of recent research investigations that center on the impact of pore pressure on the mechanical properties of fault gouge materials, their shear behavior, and changes in rate of deformation.

Terzaghi's principle states that pore pressure decreases the effective stress. According to this concept, fluid pressure reduces the amount of stress needed to cause failure, enabling fracture to

occur at depths where the rock would otherwise remain stable or as deform in a ductile manner (Twiss, et al. 1992).

Change in pore fluid pressure have a direct impact on the stability of faults, both in the case of natural earthquakes and those generated by human activities. The conventional assumption based on the effective pressure law is that the fault shear strength, τ, is dependent upon the pore pressure, p, as follows.

$$\tau = \mu^{eff} (\sigma_n - p) = \mu^{eff} \sigma_n^{eff} \qquad (1)$$

From equation (1) σ_n represents the stress acting in the direction perpendicular to the fault, whereas μ^{eff} denotes the coefficient of friction (Terzaghi 1943, Hubbert 1959).

$$\sigma_n^{eff} = \sigma_n - p \qquad (2)$$

The effective normal stress, denoted as σ_n^{eff}, is defined as the difference between the normal stress σ_n and the pore pressure p.

Fluid plays a crucial role in determining the strength of rocks and faults (Hubbert 1959). Byerlee's key research in 1978 showed that higher pore fluid pressure can reduce the effective normal stress on a fault, resulting in a decrease in frictional resistance to sliding (Byerlee 1990). Moreover, increasing pore pressures within fault zones, caused by a gradual reduction in permeability, reduce the strength of the fault and facilitate movement, even when the fault is oriented in an unfavorable orientation (Sibson 2000, Mitchell et al. 2006) and the presence of excessive fluid pressure can cause a change in the type of deformation, changing from cataclastic flow to frictional sliding. Cataclastic flow is a geological process associated with the deformation of rocks and faults. (Rawling, et al. 2001, Bense et al. 2013).

2.6 Numerical modeling

Numerical modeling is currently efficient in numerous geomechanics and rock mechanics fields, offering useful insights and helping in the design and study of complicated mechanisms in

engineering fields. In the field of geomechanics, numerical modeling is used to examine the mechanical behavior of structures, permeability, and fluid movement in soil and rock formations. The development of computer codes made a significant contribution to the development of computational mechanics, which is widely used in geomechanics. Specifically, the main approach is partial differential equations, which are used for engineering problems and related rock mechanics fields. Numerical modelling is used for the analysis of rock and soil behavior in geomechanics projects and plays a crucial role in conducting feasibility studies for underground storage projects, including carbon capture and storage (CCS) and nuclear waste disposal in the presence of high stress conditions.

FEM analysis is the most famous and widely used in the geotechnical and geomechanics fields in large deformation analysis and accurately simulates complex behaviors such as plasticity and hyper elasticity behavior, which are common in geological materials. FGMs are complex geological materials with different material properties and a range of particle sizes, shapes, and in high depth with complex stresses of overburden.

This makes it difficult to accurately simulate their mechanical response to stress using simpler analytical techniques. For the purpose of simulating of high normal loading and shear the FGM zone, modeling on Abaqus FEM of gouge material is ideal choice. Abaqus CAE (Computer-Aided Engineering) is the most powerful FEA analysis, which is very popular for numerically solving problems arising in engineering and to simulate complex real-world problems.

The domain of numerical modeling of fault gouge material is enormous and includes various areas of study in geomechanics. The study conducted by (Mair, et al. 2008) uses three-dimensional numerical simulations to investigate the evolution of fault gouge during shear. The models accurately follow the changes and behaviors of the gouge materials. Frictional-viscous flow of simulated fault gouge caused by the combined effects of phyllosilicates and pressure solution by (Bos, et al.2000) explores the frictional-viscous flow in fault gouges, highlighting the significant impact of phyllosilicates and pressure solution on the flow mechanisms within fault gouges.

2.6.1 Abaqus FEM Analysis

For Geomechanical boundary value problems in geosciences and structural studies, Abaqus software offers an extensive range of tools that help with solving of geomechanical boundary value problems in engineering.

Therefore, in Abaqus CAE, geomechanical boundary value problems can be solve with using various methodologies.

- Implicit Finite-Element Method
- Explicit Finite-Element Method
- Coupled Eulerian-Lagrangian method

Firstly, the implicit Finite-Element Method, which is capable of solving boundary value problems with small deformations with or without pore water pressure, The second approach is the explicit Finite-Element Method, which can solve boundary value problems with moderate to large deformations but is limited to single-phase analysis. Lastly, there is the coupled Eulerian-Lagrangian method, which is also capable of solving boundary value problems with large deformations but is also restricted to single-phase analysis. Moreover, to explain more precisely, single phase analysis refers to the concept that a material consists only of a single phase, such as a solid part in Abaqus, which could be in soil or rock parts, without taking into account the existence of pore fluid pressure, such as water, air, or gas, within the solid material (Pichler, et al. 2012).

Table 2-4: Engineering applications of the Finite Element Method (Rao 2017)

Area of Study	Equilibrium Problems	Eigenvalue Problems	Propagation Problems
Geotechnical Engineering	Static analysis, beam, shear loading walls, and concrete structures.	Natural frequencies and stability of structures	Propagation of stress waves and moving particles moving in the structures.
Geomechanics Field	Analysis of excavations, underground openings, rock joint, stress analysis in soils, dams etc.	Natural frequencies and soil-structure interaction problems	Seepage in soils and rocks; stress propagation in soils and rocks

To conclude the literature review on the importance and behavior of the gouge materials in the fault zones, which reveals that the fault gouge materials play a vital role in the fault slipping phenomena and seismic activity, Many researchers examine and investigate the close and complex relationship between pore fluid pressure and the mechanisms of the deformation of the fault-gouge materials. It shows how these factors greatly impact the mechanical behavior of fault zones. To study the behavior of saturated fault gouge materials by using numerical modeling on Abaqus FEM analysis, we have significantly improved our understanding of the gouge material behavior in terms of shear and normal load.

3. Methodology

3.1 Numerical modelling

The numerical modeling was conducted employing the finite element method in Abaqus CAE 2024. Utilizing Abaqus Software, a numerical model is constructed to examine the mechanical interactions and stress distributions under applied loads and boundary conditions. This model contains two steel plates and a layer of fault gouge material (FGM) between them. This setup is particularly relevant for simulating the actual conditions related to those in fault zones, where understanding the behavior of FGM under compression and shear is crucial for fault mechanics.

In finite element analysis, elements are the basic shapes that are used to divide the complicated shape into smaller pieces of different shapes that can be used to get a solution over a region. The whole area of interest has been divided up into smaller pieces, which are linked together at places called nodes. The degree of freedom of a system is usually the number of separate ways that its nodes can move. In three-dimensional space, these nodes could be translations and rotations.

The finite element method consistently follows a systematic and sequential approach for solving a generic continuum problem. The step-by-step approach for addressing static structural concerns can be outlined as follows:

- **Step 1** Divide the whole region and structure in discrete elements.
- **Step 2** The appropriate interpolation or displacement model should be chosen, and the solution of the elements that suggested should possess computational simplicity while satisfying specific convergence criteria for the elements of the nodes.
- **Step 3** Determine the stiffness matrices and load vectors of the elements.
- **Step 4** Determine the overall equilibrium equations, so it is necessary to assemble the element equations. According to the combination of several finite elements, it is necessary to build the stiffness matrices and load vectors of each element appropriately. So the overall equilibrium equations must be established.

$$\sum_{j=1}^{N} \quad \left(\left[K \frac{e}{ij} \right] \left(u \frac{j}{i} \right) = \sum_{j=1}^{N} \quad \left(f \frac{e}{j} \right) \right. \tag{1}$$

$$[K]u = F \tag{2}$$

From the above equation, where matrix $[K \frac{e}{ij}]$ is the coefficient matrix, vector $[u \frac{j}{i}]$ is the nodal value vector of unknown variables, and the vector $[f \frac{e}{j}]$ is comprised of contributions from body force terms and initial boundary conditions. For elasticity problems, the matrix$[K \frac{e}{ij}]$ is called the element stiffness matrix.

- **Step 5** Solve the above equation for the unknown displacement
- **Step 6** Compute and find the elements stress and strain analysis by using the solid mechanics equations.

3.2 Abaqus CAE Software FEM Analysis

The Abaqus software is a powerful finite element analysis (FEA) software that is widely used in many engineering fields, such as geomechanics and geotechnics, for the purpose of simulating the reaction of soil and rock to predict the behavior of the solid materials under different mechanical loads.

3.2.1 Model Setup for the simulation

ABAQUS version 2024 has been chosen as the primary tool for Finite Element Method (FEM) analysis due to its versatility and suitability for simulating the pore fluid pressure analysis for gouge materials. ABAQUS is a highly trusted and commonly used software package for finite element analysis (FEA) developed by Dassault Systèmes Simulia Corp. The software ABAQUS enables the modeling of complex physical processes, providing engineers and researchers with a digital platform for evaluating the performance of structures and solid materials. The typical sequence of the simulation in ABAQUS is given below.

- Domain discretization

- Assigning materials properties
- Assemble the model
- Applying boundary conditions
- Model's contact interaction
- Stepping the model to solution
- Apply Loading and boundary condition
- Meshing the model
- Job and result analysis

3.3 Geometry of the Model

The geometry for the model was choose to replicate the large shear box dimension which designed for the experimental test. The shear box design is complete, with remaining efforts concentrated on finalizing cost estimates and securing the budget required to commence the experimental phase. This will ensure the validation of the geometry used in the numerical simulations.

3.3.1 Large shear box design considerations

For the experimental phase of our study on the mechanical behavior of fault gouge material (FGM) under influence fluid, a large shear box apparatus has been carefully designed. The large shear box, with the dimensions of 60 cm by 30 cm by 25 cm, is specifically designed to enable the measurement of mechanical reactions of FGM. This setup includes an advanced hydraulic loading system to apply both normal and shear stresses accurately, to replicate subsurface pressure conditions experienced by geological formations.

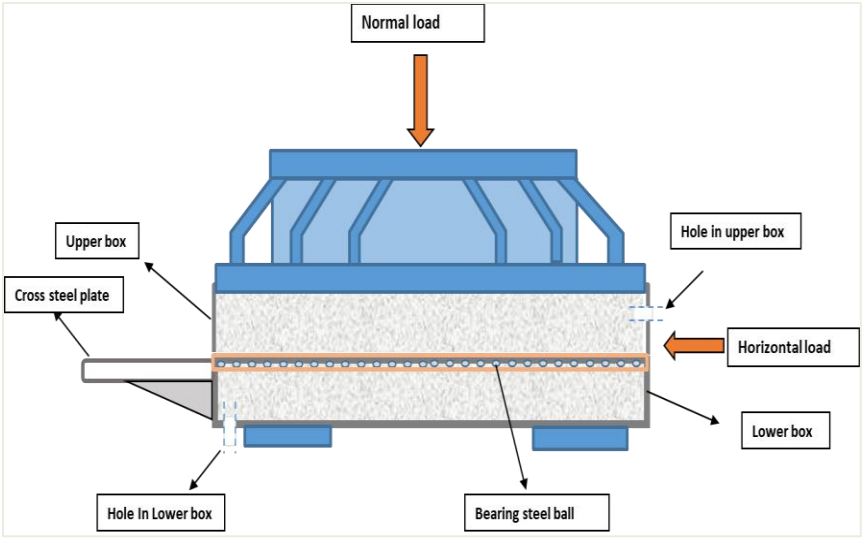

Figure 3-1: Schematic view of large shear box design

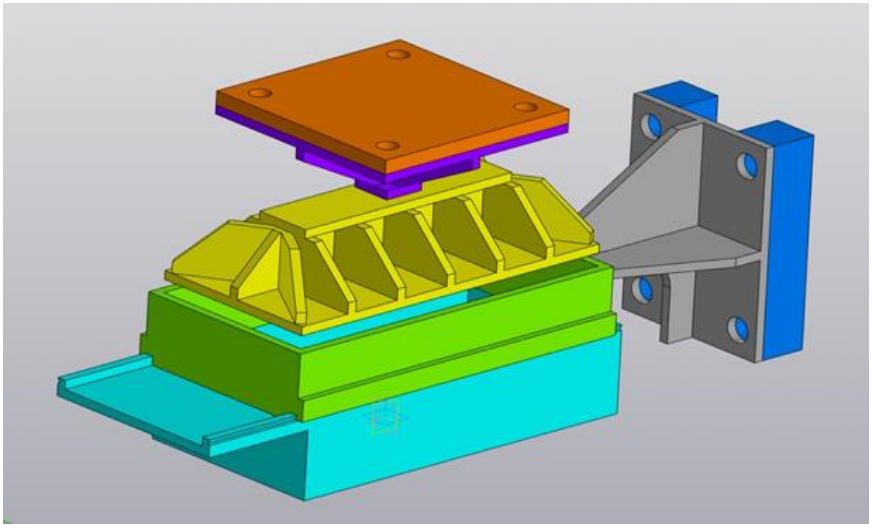

Figure 3-2: Initial design of large shear box

This extensive shear box setup is an essential tool for connecting numerical simulations with the real mechanical behavior of (FGM). It provides empirical data that supports the accuracy of simulation results in both academic research and practical applications in geotechnical engineering.

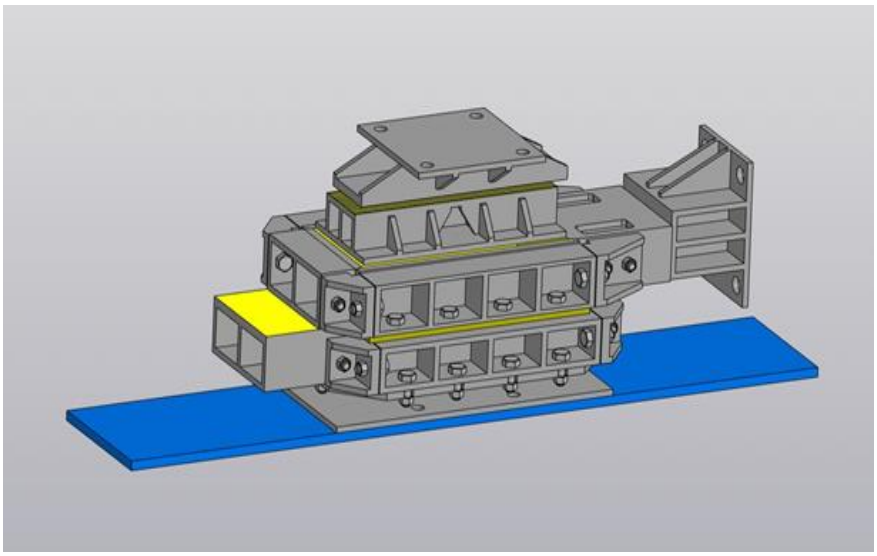

Figure 3-3: Final engineering design of large shear box

The design of the large shear box is already complete, with pending work focusing on finalizing the details of cost estimation and budgeting to start the experimental work to ensure validation of the choosing geometry for the numerical modelling simulation. This setup and design can replicate the complex interplay between geological materials and fluid pressures. It will significantly enhance our understanding of FGM mechanical and dynamics behavior and serve as a valuable tool for testing and validating simulation results within academic research.

The model design has been selected to precisely replicate the dimensions of the shear box, this will enable a direct comparison between the numerical results and experimental data once the shear box is in utilize. The numerical simulation involves placing the fault gouge material (FGM) between two steel plates, which models the mechanism of a shear box. This set up allows the FGM zone to go through both normal and shear loads. It is essential for validating the simulated mechanical behaviors of FGMs, such as stress distribution, strain, and permeability analysis

The model includes three separate parts. The geometry of the model consists of a 5 cm-thick gouge material positioned between two steel plates. The upper steel plate has a measurement of 3 cm, while the lower plate is 7 cm. The overall length dimensions of each component of the model are 60 cm by 30 cm. The chosen geometry for the FGM between two steel plates is carefully chosen to replicate the natural fault zones while effectively handling computational complexity and focusing on essential interactions. The design geometry aims to look at fault

gouge dynamics under shear and normal stresses, which allows us to conduct a comprehensive investigation of the deformation mechanisms of FGM in the fault zone.

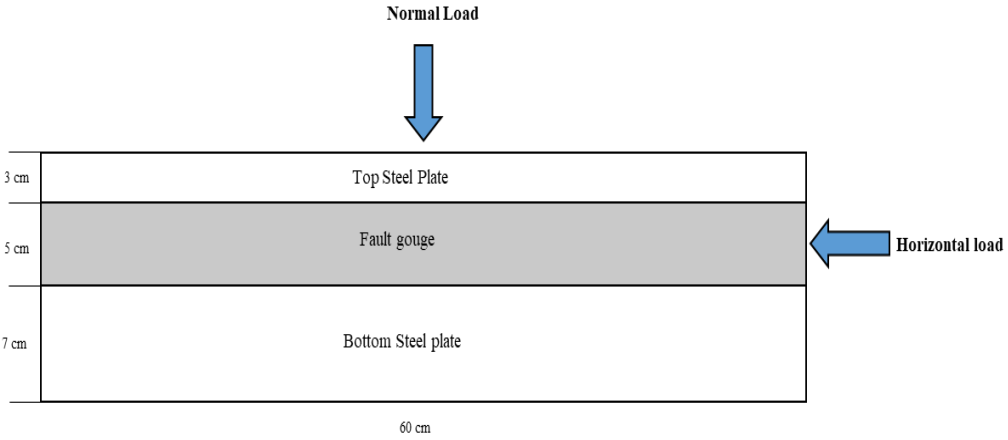

Figure 3-4: Geometry of the model built within ABAQUS environment

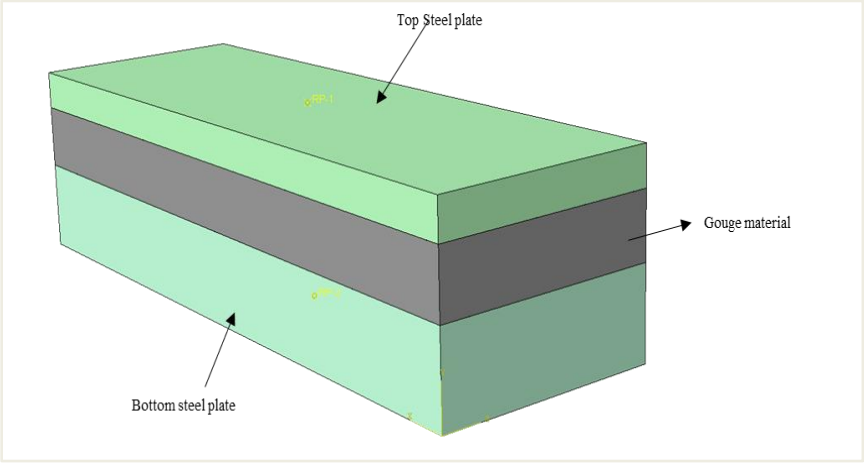

Figure 3-5: 3D view of the model geometry

3.4 Material properties

Two different models, namely an elastic model and a Mohr-Coulomb plasticity model, were simulated independently within the implicit/explicit modeling framework of Abaqus. Each model's material properties were carefully established and adjusted based on the specific elastic and plasticity criteria for each model. Based on reported literature data, the following properties were compiled from the available data and used as input data in the modeling exercise: The input data is presented in Tables 3.1 and 3.2

Table 3-1: Average input properties of fault zone gouge materials used as input

Property	Average Value	Conditions	References
Permeability (k)	10^{-10} to 10^{-22} m²	Highly dependent on clay content	Lockner (2009) Faulkner (2010)
Young's Modulus (E)	0.01 GPa	Varies with mineralogy and confining pressure	Treffeisen (2020)
Poisson's Ratio (ν)	0.2 to 0.3	Depends on composition and porosity	Faulkner et al. (2006)
Coefficient of Friction (μ)	0.3-0.45	lower in the presence of fluids and clay minerals	Byerlee (1978)
Pore Pressure	Variable		Zhang (2019)

The properties for the elastic model fall under Hooke's law, which describes deformation in the elastic domain by establishing a relationship between stress and strain through an elasticity (or stiffness) matrix. If the material behavior is linear-elastic and isotropic, it is sufficient to consider only two material properties: Young's modulus and Poisson's ratio. The Young's modulus, also known as the modulus of elasticity, Table 3.2 shows the elastic model properties for the fault-gouge materials..

Table 3-2: Elastic model input properties

Property	Fault Gouge material	Steel plates
Density (kg/m3)	1990	7800
Young's Modulus (GPa)	0.035	200
Poisson Ratio	0.3	0.28
Permeability ($m^{2)}$	1e-10	-
Void ratio	0.6	-

Table 3.3 below shows the details of the f the properties used in the numerical model based on Mohr Coulomb's plasticity. The outline consists of mechanical properties with parameters that

define the plastic behavior of the FGM, such as angle of internal friction, dilation angle, and cohesion yield stress. These parameters are essential to looking at the volumetric change upon shearing the materials.

Table 3-3: Mohr Coulomb's plasticity Model properties:

Property	**Fault gouge material**	**Steel plates**
Density (kg/m3)	1990	7800
Young's Modulus (GPa)	2	200
Poisson ratio, v	0.3	0.28
Permeability	1e-15	-
Void ratio	0.4	-
Mohr coulombs Plasticity		
Plasticity	**Angle of friction**	**Dilation Angle**
	10^{o}-25^{o}	10^{o}-15^{o}
Cohesion	**Cohesion Yield Stress**	**Abs Plastic Strain**
	70000 Pascal	0

3.5 Stepping the model to solution

In Abaqus, the step module is used as the platform for defining the analysis technique employed in a simulation work. Each step represents an individual phase of the physical process to simulate, such as the act of loading and unloading. The combination of two separate steps for normal and horizontal loading represents an appropriate and systematic methodology for the sequential application of various loading circumstances for modeling.

The following defining steps for both models in the simulation are as follows:

1- First Soil Step for normal loading

In the first soil step, the initial step was to apply the normal or vertical load to the top of the steel plate. The primary objective of this step is to calculate the overburden pressure that the materials experience in their actual condition.

2- Second Soil Step for Horizontal Loading

The second soil step applies to the horizontal movement to shear the FGM between two steel plates. The primary objective of this step is to investigate shear strength, slipping surface, and the material's response to combined normal and shear stresses.

For FGM modeling, both soil steps have been used, which is more suitable for the specific soil type and offers more accurate outcomes for the gouge materials. In both steps, it is necessary to establish the boundary condition and loading conditions, as discussed in the next sections on loading conditions and boundary constraints.

For each step, the details of the convergence criteria used for the solution of each step, including tolerances for loading and displacement of the elements.

3.6 Model's contact interaction

Model contact interaction is very important when dealing with different model parts that come into contact with each other during the analysis. It has a vital role because these interactions are essential for precisely replicating the real-world behavior of materials in contact, especially when utilizing numerical modeling. In the geometry setup of a model including steel plates and FGM, it is needed to define the contact interactions between the surfaces of the steel plates and the gouge material.

The general interaction has been applied between FGM and steel plates to capture the physical phenomena of the interaction between these parts of the materials. To define the interaction properties of the materials, two types of behavior are considered within the Abaqus contact logic:

- Shear behavior
- Normal behavior

For shear behavior, a friction coefficient of 0.4 was selected on the basis of literature data that represents the resistance to sliding between the steel and gouge materials when subjected to a load. The coefficient of friction plays an important role in determining the distribution of shear stress and the probable sliding behavior at the contact.

The ‘Hard contact’ has been selected for the normal behavior of the interaction between steel plates and the gouge material because it represents the contact pressure response for parts when they are pressed against each other. The use of this setup provides the absence of any infiltration between the gouge material and the steel surface when subjected to compression, therefore simulating an actual physical constraint that occurs in engineered systems.

3.7 Implementing Boundary and Loading Conditions

The loading conditions and boundary constraints for both numerical models, which include fault gouge material and steel plates, are presented in Tables 3.4 and 3.5. The table specifies the parameters for axial loading, shear displacement, and mesh in detail.

In the elastic analysis, a normal load of 4 MPa was applied in the first soil step, and a 1 MPa pore pressure boundary condition was applied, designed to simulate the fluid movement within the gouge materials. The introduction of pore pressure was applied from the right side, serving as an inlet, and then propagated through the model (FGM) until it exited on the left side, providing an outlet for fluid movement. While maintaining the initial normal pressure at 4 MPa, the model generated an extra shear displacement of 5 cm in the second soil step. This was done while maintaining the same level of axial stress.

Table 3-4: Elastic model loading and boundary condition

Loading condition	Values	Boundary Condition (BC)
Normal Loading	4 MPa	With axial load on top plate the BC is allowed downward (-Y-axis)
Shear displacement of the gouge	5 cm	With shear load the BC for top plate is allow 5 cm (-X-axis) moving horizontally.
Gouge Material	5cm (height)	
Mesh Size	0.5 cm	
Total Elements	6000	
Top and Bottom steel	3 cm +7 cm = 10 cm (h)	The BC for Bottom Plate is set fix from all direction.
Mesh Size	2 cm	
Total Elements	1800	
Pore pressure	1 MPa	Inlet from right side and outlet from left side

In the conducted plastic analysis, the Mohr Coulomb model was used, an axial load of 1 MPa was applied in the first soil step, and a 0.01 MPa pore pressure was integrated, designed to simulate the fluid movement within gouge materials. The introduction of pore pressure occurred from the right side, serving as an inlet, and then propagated through the model until it exited on the left side, providing an outlet for fluid movement. A shear displacement of 2 cm was imposed on FGM under the applied confining stress while keeping the initial axial stress constant at 1 MPa. The boundary conditions about pore pressure were maintained consistently with the initial step, enabling a continuous evaluation of the influence of fluid dynamics on the properties of the material.

Table 3-5: Mohr coulomb plasticity model loading and boundary condition

Loading Condition	Values	Boundary condition (BC)
Normal Loading	1 MPa	With normal load on top plate the BC is allowed downward (-Y-axis)
Shear displacement of the gouge	2 cm	With shear load the BC for top plate is allow 2 cm (-X-axis) moving horizontally.
Fault Gouge Material	5 cm (height)	
Mesh Size	0.5 cm	
Total Elements	6000	
Top and Bottom steel	3 cm +7 cm = 10 cm (h)	The BC for Bottom Plate is set fix from all direction.
Mesh Size	2 cm	
Total Elements	1800	
Pore pressure	0.01 MPa	Inlet from right side and outlet from left side

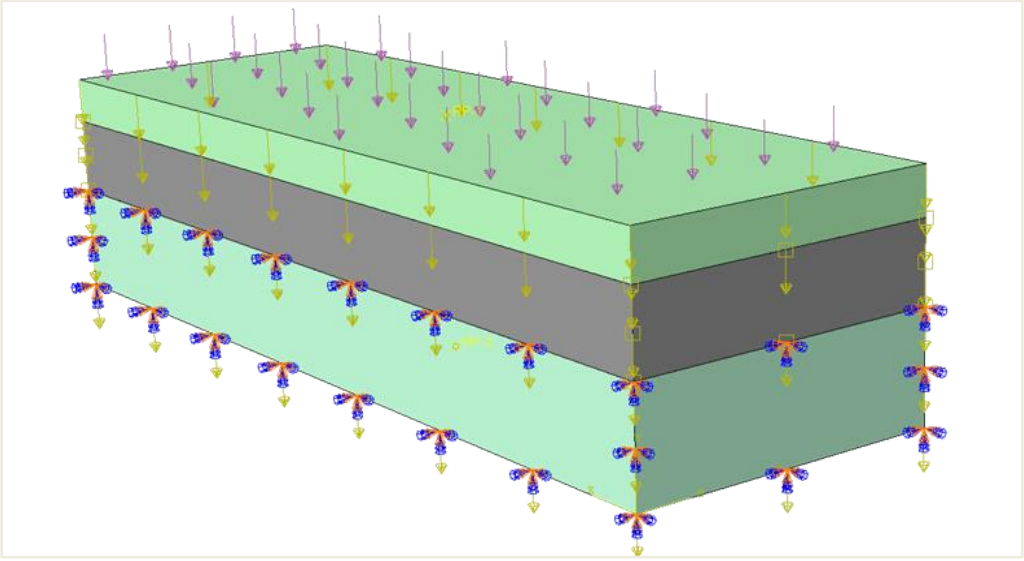

Figure 3-6: Abaqus CAE loading and Boundary constraints

3.8 Model discretization

3.8.1 Mesh sensitivity analysis

When performing the mesh sensitivity analysis, it's important to find the ideal mesh size that accurately simulate the stress strain distribution in the finite element model, while considering computational efficiency into account for it. For the FGM zone, three different mesh sizes were considered: 0.8 cm, 1 cm, and 1.2 cm.

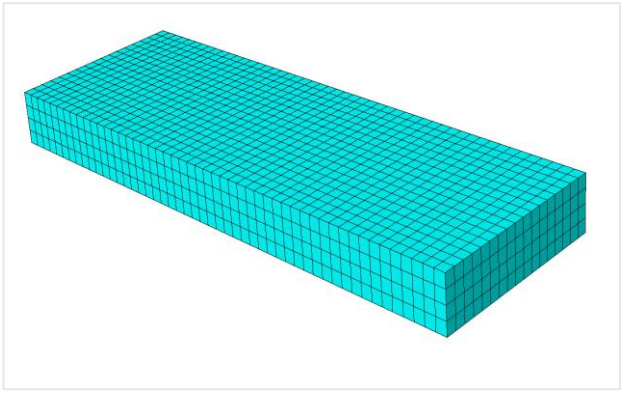

Figure 3-7: Discretization of FGM zone using an element size of 1.2 cm

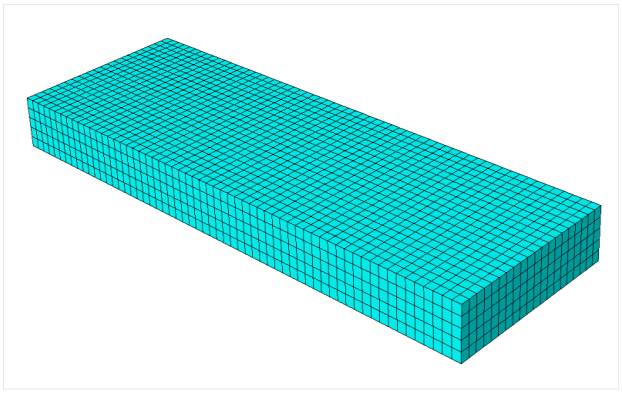

Figure 3-8: Discretization of FGM zone using an element size of 1 cm

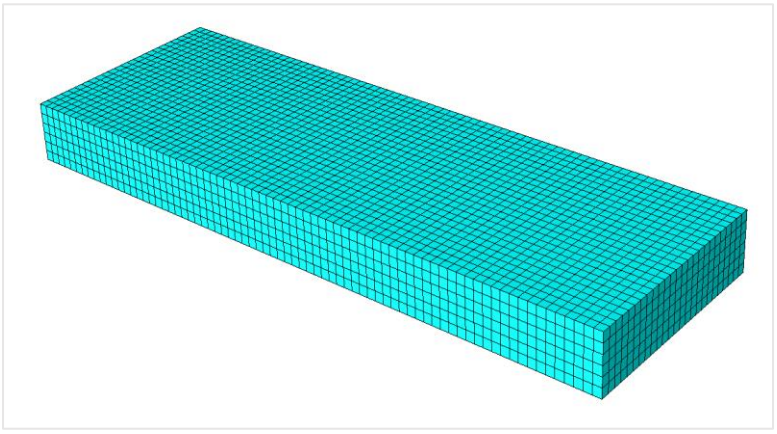

Figure 3-9 Discretization of FGM zone with an element size of 0.8 cm

In the FGM zone, three different mesh sizes were tested including 1.2 cm with 3,400 elements, 1 cm with 6,000 elements, and 0.8 cm with 11,250 elements. The 1 cm mesh size was selected for the simulation, getting a balance between detail and computational efficiency. While the 0.8

cm mesh offered higher resolution, it required significantly more computational power, making the 1 cm mesh a more practical choice for this simulation.

3.8.2 Mesh Sensitivity Analysis Outcomes

After observing the resulting deformation behaviors of FGM zones, we can see from the contour plots that the strain distribution is the same considering how fine the mesh is. This type of consistency leads to a convergent solution, which means that refining the mesh even more doesn't make a big difference when the computer simulates the mechanical response of the material. In particular, the contour plots for mesh sizes of 0.8 cm and 1 cm show similar. This suggests that the model's reaction is well-defined at these levels of detail meshing of the FGM zone.

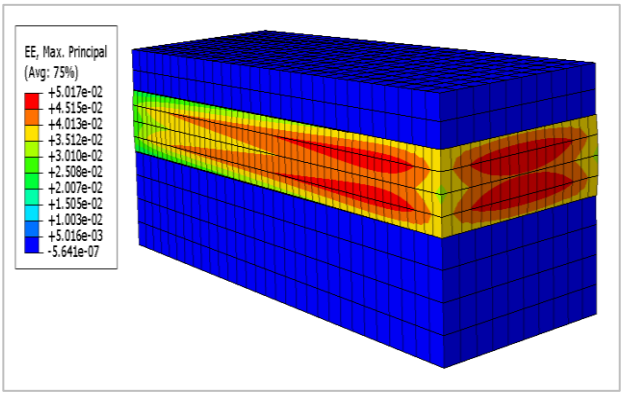

Figure 3-10 Max Elastic Strain distribution in (FGM) zone with a discretization of 1.2 cm

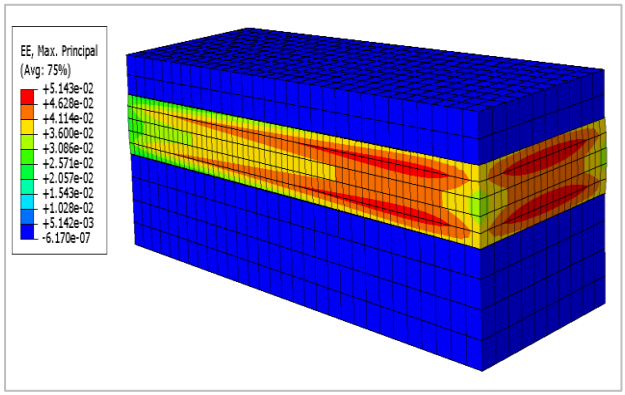

Figure 3-11: Max Elastic Strain distribution in (FGM) zone with a discretization of 1 cm

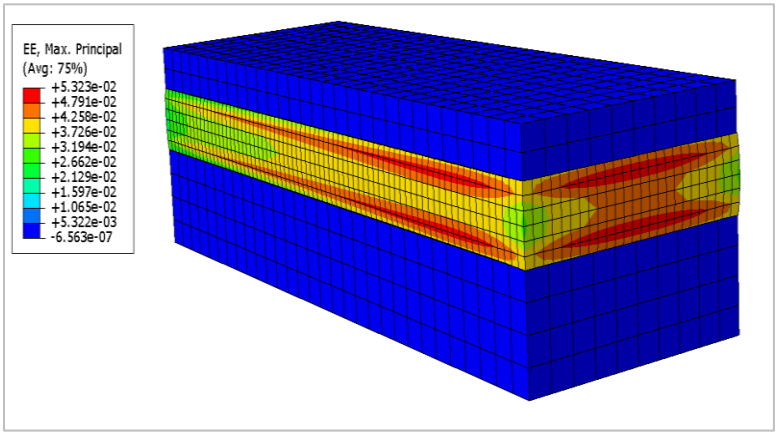

Figure 3-12: Max Elastic Strain distribution in (FGM) zone with a discretization of 0.8 cm

The mesh size of 1 cm, therefore, is an appropriate choice for numerical simulation. The choice was made based on two primary considerations: computational simplicity and accuracy of the simulation results for FGM zone. The small difference between the results for the 0.8 cm and 1 cm meshes suggests that the smaller mesh is not significantly better at getting the mechanical behavior of FGM under the current loading conditions. On the other hand, using a 1 cm mesh fits with the need for computational difficulty.

3.8.3 Optimal mesh for model segmentation

For accurate model discretization, choosing the right mesh size is very important. It affects both the precision of the results and the computational efficiency. In the previous section, we investigated the sensitive analysis, to determine the optimal mesh setup for our model. We examine by looking different mesh sizes and their corresponding effects on model accuracy and performance.

This process is followed in the model separately for each part, and the details of the element size and number are different for FGM and steel plates. We divided the 5 cm-high gouge material layer into elements using a mesh size of 1 cm. The FGM was meshed using a total of 6,000 elements, as shown in figure 3.4. The utilization of a high-density mesh in the simulation results of the gouge material guarantees a heightened level of accuracy, enabling a comprehensive examination of its mechanical responses.

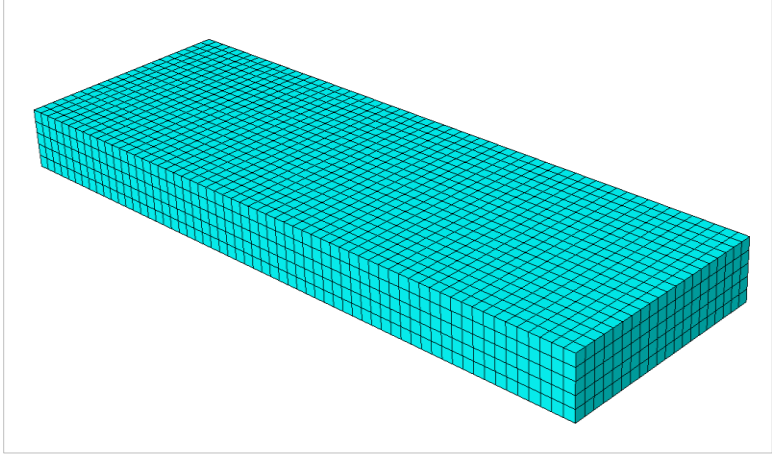

Figure 3-1: Gouge material discretization (element size is 1 cm)

Meshing is also done for both steel plates at the top and bottom of the FGM. The steel plates, with dimensions of 60 * 30 * 10 cm, were given a mesh with a relatively large size, with each element measuring 2 cm. The use of a coarser mesh in this context indicates that the steel plates are given less analytical attention compared to the fault gouge material (FGM) and have the least interest area for the result analysis. In total, 1800 elements for both steel plates were generated, which will effectively balance the computational efficiency with more accurate results from the simulations.

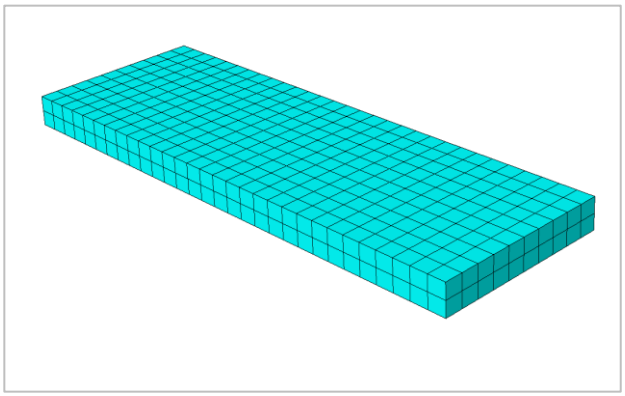

Figure 3-2: Top steel plate meshing

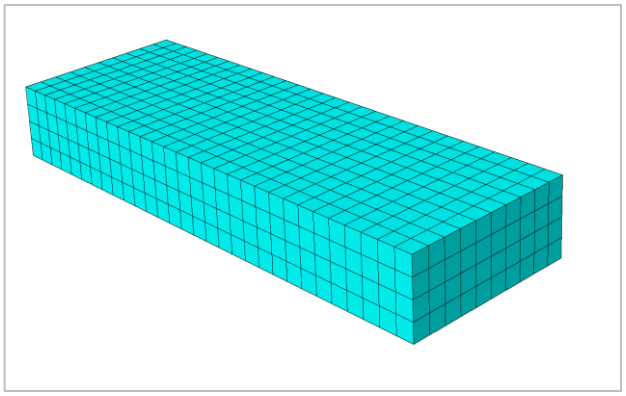

Figure 3-3: Bottom steel plate meshing

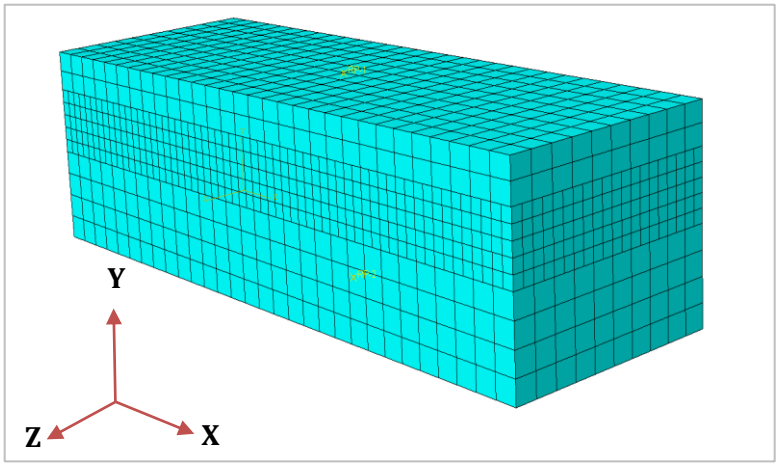

Figure 3-4: Complete model discretization scheme

Following the methods and processes previously outlined, it is necessary to execute and implement the model for job analysis. This requires precisely defining all geometrical measurements, material properties, meshing, boundary, and loading conditions to ensure they accurately reflect the proposed physical conditions.

4. Results and Discussion

This section of the thesis discusses the results of the finite element method simulation, which was conducted with the help of the Abaqus FEM. The purpose of these simulations is to investigate the effects of confining and shear loading on the mechanical behavior of fault-gouge materials with and without pore pressure. The most important part of the simulation is to examine how fluid pressure influence the deformation rate and shear response of the gouge materials.

By conducting numerous simulations, the presented results offer a good understanding of the mechanical behavior of fault gouge materials and the relationship between pore pressure and deformation rate. This research significantly enhances our understanding of fault gouge mechanics but also has practical implications for predicting and minimizing geotechnical risks related to fault movement associated with CCS projects.

4.1 Elastic Analysis

Elasticity models are fundamental in engineering work because they describe how materials deform under stress and how they return to their original position after removing stress or unloading the materials. The main goal was to evaluate the initial stiffness, distribution of stress in the FGM zone, and deformation rate of the material in its elastic condition. Table 4.1 provides the input parameters for the elastic model.

Table 4-1: Elastic Model input properties

Input Properties of FGM	**Values**
Density (kg/m3)	1990
Young's Modulus (GPa)	0.035
Poisson Ratio	0.3
Permeability (m^2)	1e-10
Void ratio	0.6

The first analysis is to examine the elastic response of fault gouge material (FGM) under normal and shear loading conditions.

4.1.1 Pore Pressure

In the first soil step for normal loading, a 4 MPa load applied vertically to the top steel plate while the bottom plate is fixed from all sides. The fault gouge materials are sandwiched between the two steel plates and shear the fault gouge material 5 cm horizontally in the second soil step while the pore fluid pressure of 1 MPa were applied for both steps. The pore pressure propagates from the right to the left side within the fault gouge material, as shown in figure 4.1.

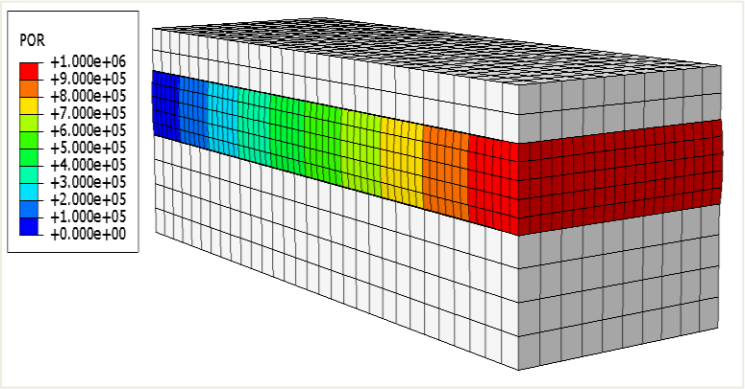

Figure 4-1: The propagation of pore pressure from right to left within the model.

Within the framework of Abaqus, the visualization module's contour plots commonly indicate the average value for the output parameter over a certain element or region of interest. To investigate and look at the pore pressure in the FGM zone, the focus on a central node point shown in the Figure 4.2 was selected. This point serves as a precise location to check the pore pressure propagation in the simulation with an accurate graphical representation, as shown in figure 4.3.

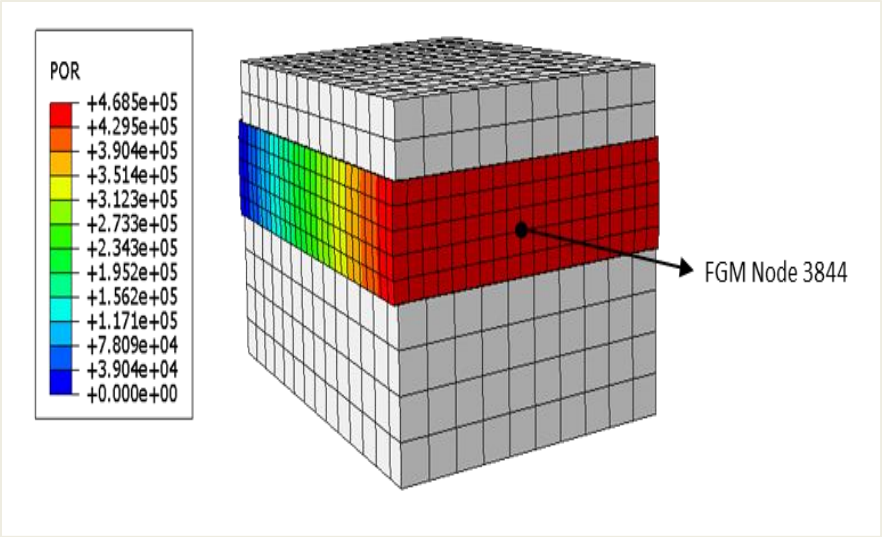

Figure 4-2: The selected central nodal point in FGM zone

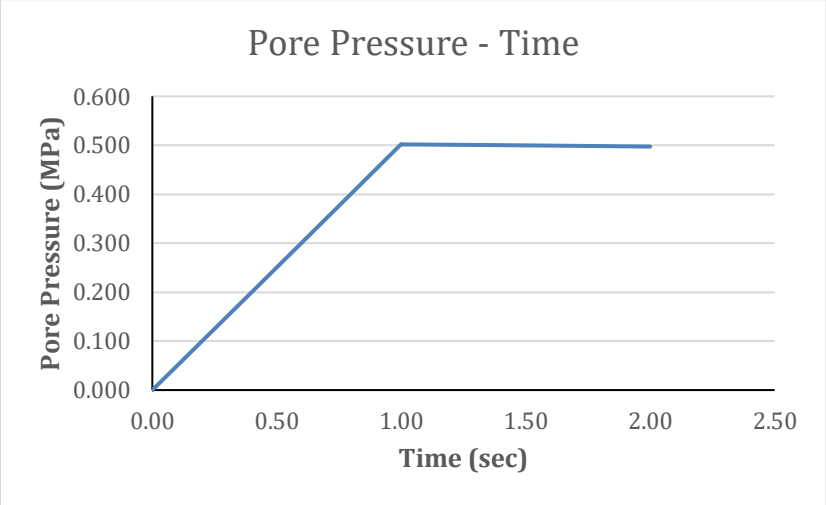

Figure 4-3: Pore pressure propagation with respect to time at central Node 3844

The pore pressure graph at the selected node 3844 in the central FGM zone represents the pore pressure against time. The pore pressure reaches its maximum value of 0.5 MPa in the first soil step normal load condition and remains the same for the second soil step shear load condition, which indicates that no changes occur in the pore pressure in the second horizontal shear loading step.

4.1.2 Total Fluid Volume Ratio (FLUVR)

Total Fluid Volume Ratio (FLUVR), which measures the fluid presence within the FGM zone, is the most important parameter that affects the mechanical properties of the fault gouge material. Within the framework of ABAQUS and the visualization module's contour plots, "(AVG: 75%)" commonly indicates the average value for the output parameter over a certain element or region of interest.

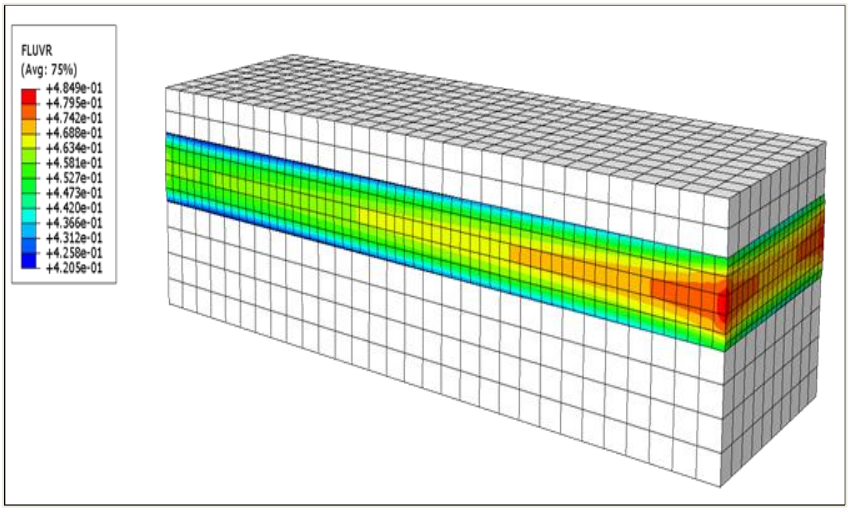

Figure 4-4: Total Fluid Volume Ratio (FLUVR), show the volume of fluid within the FGM

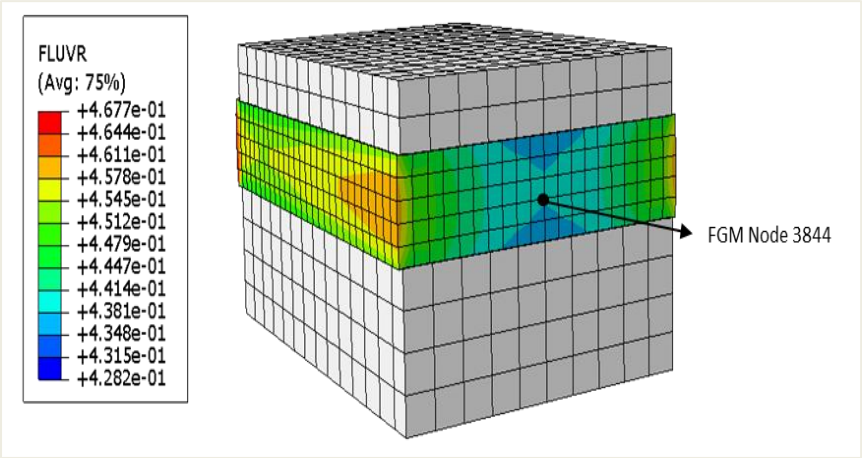

Figure 4-5: FGM central unique Node 3844

In the material of the fault gouge, the total Fluid Volume Ratio (FLUVR) is shown in Figure 4.6 throughout a period of time at a particular central node, which is central nodal point 3844 of the FGM.

.

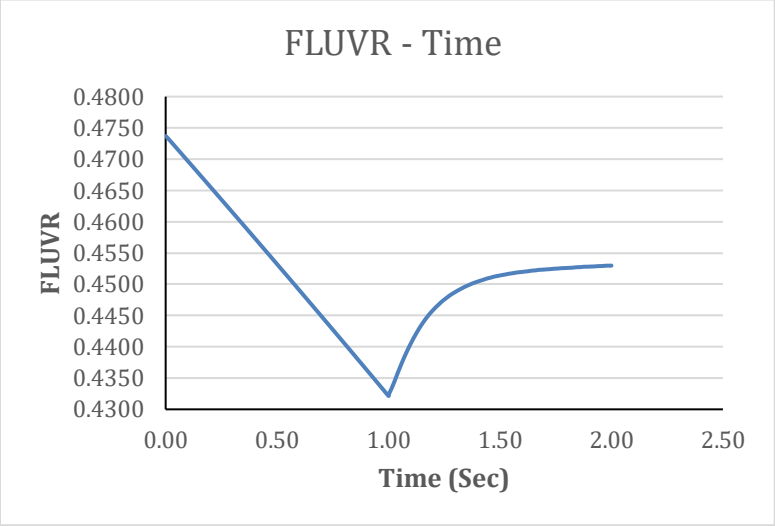

Figure 4-6: Total Fluid Volume Ratio (FLUVR) over time at a central FGM nodal 3844

The graph shows an initial decrease in FLUVR from around 0.47, reaching its minimum at approximately 1 second, and increasing above the 1.5-second level.

After the initial reduction in the FLUVR in the first step by applying normal loading, there is an increase in the second shear step in the FLUVR. Which indicates that the volume of fluid at this node is rising again. This increase may be caused by the shear forces applied to the gouge materials during the horizontal movement of 5 cm in the second step, or it could be an effect of a of a decrease in the compaction rate because of the shear movement. As a result of the applied pressure, this behavior is a reflection of the dynamic changes that occur in the presence of fluid within the fault gouge.

4.1.3 Stress-strain Analysis

The elastic model provides a 3D representation of stress distribution within the fault gouge material under applied loading, as illustrated in figures (4.7–4.9). These figures show a visual distribution of the elastic strain experienced by the fault gouge materials by applying a normal load of 4 MPa to the elastic model under the influence of the pore pressure. The color counter plot shows the magnitude of the elastic stain quantity within the fault gouge material. The most intense is in the central right region of FGM, which suggests that this area is experiencing the

most deformation, which is the focus area for our analysis to extract the data for stress strain analysis.

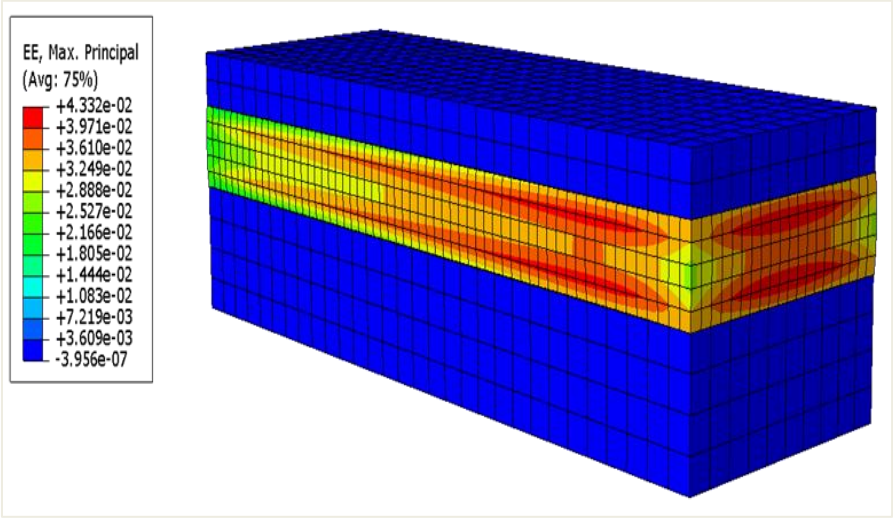

Figure 4-7: Elastic strain distribution under the influence of pore pressure

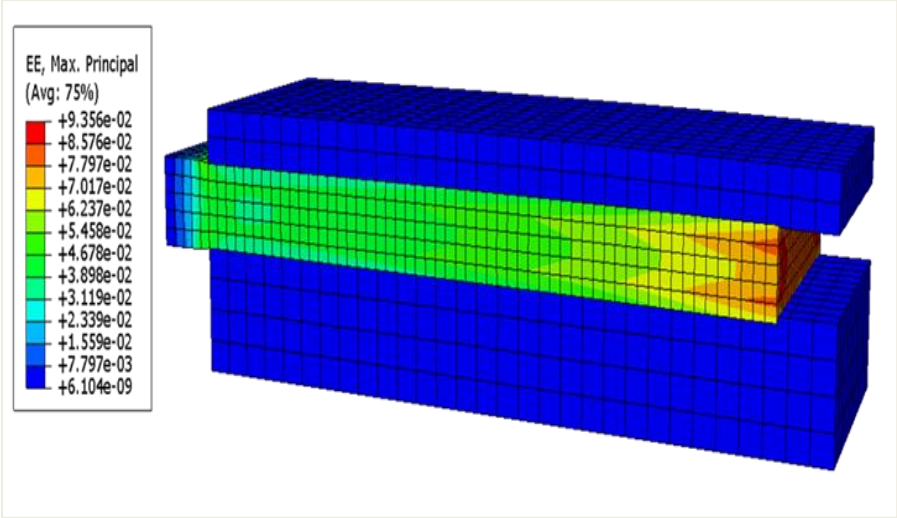

Figure 4-8: Elastic strain distribution at 5 cm horizontal movement

Figure 4.9 shows the relationship between stress and time for a fault gouge material (FGM) at a specific location that is denoted by the FGM node 3844. It illustrates how the stress level alters over an interval of 2.5 seconds at this particular point in time. At first, the stress level rises rapidly with the passage of time, reaching its highest peak point of 3.64 MPa in one second. Immediately after this peak load, the stress does not significantly increase and remains reasonably stable with a minor decrease in the second step, where the FGM is horizontally sheared by 5 cm. This

behavior indicates that the material reaches a failure mode after shear displacement, as demonstrated by the fall in stress, which may imply that the material has begun to fail and yield as a result of the shearing.

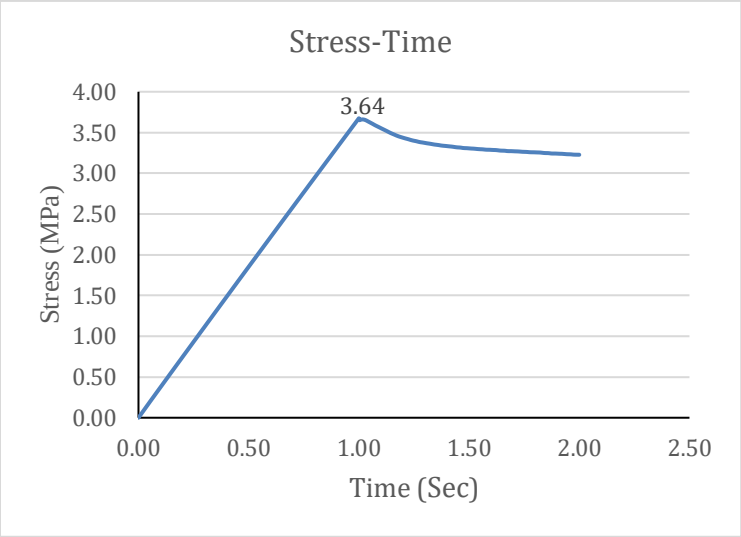

Figure 4-9: Stress-Time relationship for FGM at central node 3844

The graph shows the stress-strain relationship for FGM at specific node 3844 to indicate the material response to the applied load. Initially, the curve displays a straight line, indicating that the material has experienced elastic deformation and can regain its original shape upon removal of the load. The yield strength is the highest stress that a material can handle before it starts to break. It is about 3.65 MPa. The small drop in the curve after the peak indicates the FGM's failure mode and the onset of plastic deformation, potentially due to strain hardening.

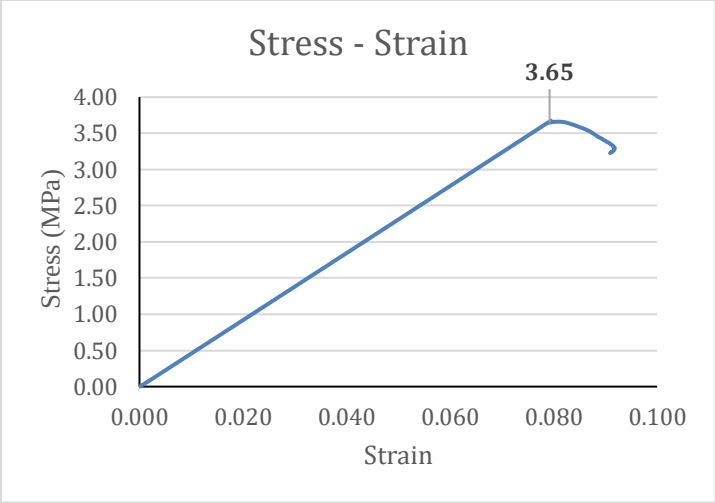

Figure 4-10: Stress-strain relationship for FGM at central node 3844

4.1.4 Total Displacement

In the context of Abaqus, the symbol "U" indicates the output of the displacement field and is used as a representation of the displacements of nodes within the model. To be more precise, the symbol "U" represents the overall displacement vector for every node. The three components for displacement are denoted as U1, U2, and U3, which correspond to the displacements in the X, Y, and Z directions, respectively. The total displacement is important in understanding the behavior of the model when subjected to imposed stresses or boundary conditions. This approach can be used in order to assess the total deformation of the structure.

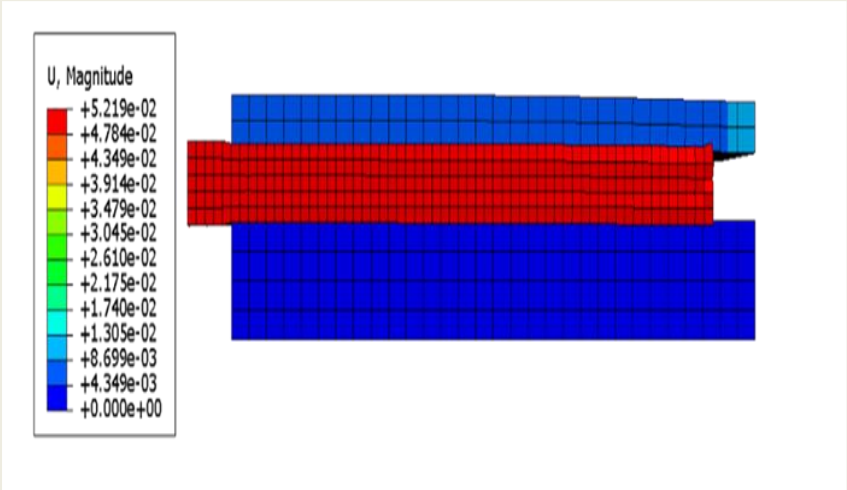

Figure 4-11: Total displacement of FGM in elastic analysis

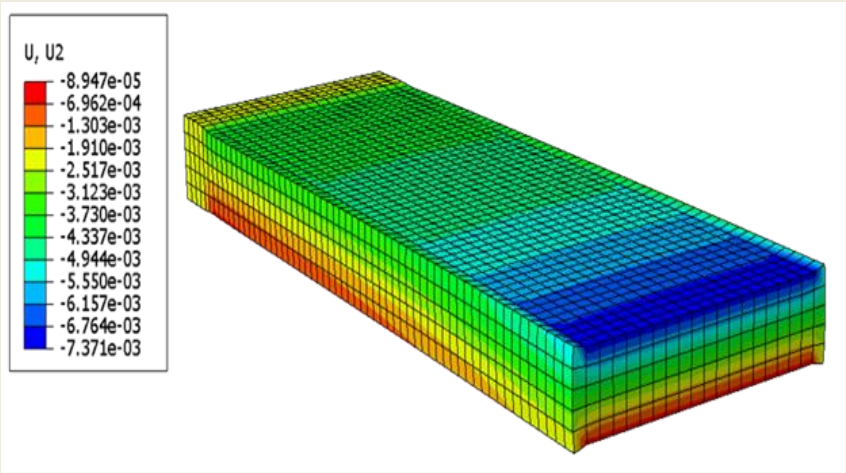

Figure 4-12: Total Displacement (U2) of the FGM in Mohr-Coulomb plasticity model

The elasticity model for Fault Gouge Material (FGM) is obtained by applying a normal load of 4 MPa and a horizontal shear displacement of 5 cm, as shown in figure 4.11. The model is run with these loading values because of the computational capacity of the computer. The contour plot just shows the total displacement of the FGM.

However, figure 2.12 illustrates a more specific look at the FGM material "U2" compaction between the steel plates, where the contour plot indicates the value range from 0.01 cm to 0.6cm for elastic analysis.

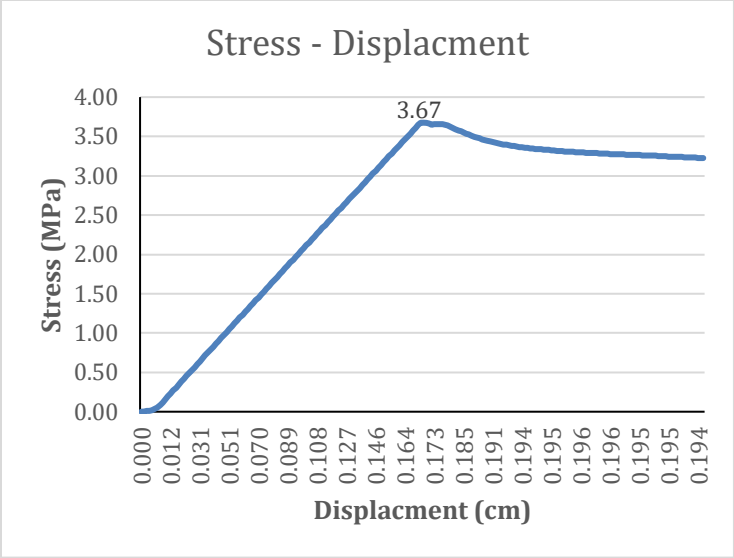

Figure 4-13: Stress-Displacement (U2) relationship FGM at central node 3844

The stress-displacement graph showing the behavior of the FGM zone at node 3844 demonstrates the changes in stress levels resulting from a horizontal displacement of 5 cm while applied to a normal load of 4 MPa. Initially, the FGM shows an elastic behavior where stress is directly proportional to the displacement, but it shows a failure mode when it reaches the yield point, where the peak stress is approximately 3.67 MPa.

4.2 Mohr-Coulomb Plasticity Model

The Mohr-Coulomb plasticity model is a basic approach in Abaqus CAE software for analyzing the yield behavior of geomaterials like soil, rock, and certain types of materials particularly when these materials are under low levels of confinement loading conditions.

For the modeling of FGM zone, the Mohr-Coulomb model was specified by different FGM material properties. These parameters include cohesion, friction angle, and dilation angle from empirical data, as well as the addition of elastic properties, as shown in the previous section, Table 3.2.

4.2.1 Pore Pressure

In the Mohr Coulombs plasticity model, 1 MPa normal load is applied vertically to the top steel plate while the bottom plate is fixed from all sides. Then move the FGM horizontally by 2 cm in

the second soil step while applying a pore fluid pressure of 0.01 MPa for both steps. The pore pressure propagates from the right to the left side within the fault gouge material, as shown in the figure 4.14.

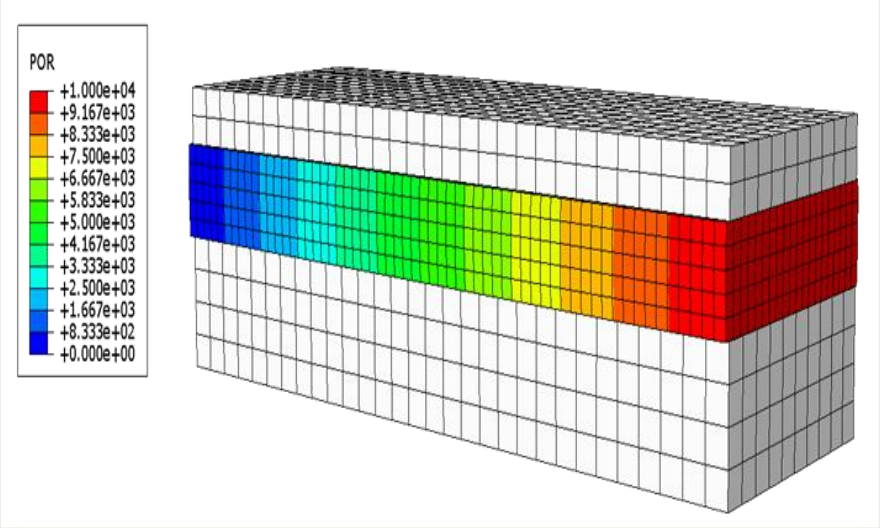

Figure 4-14: The propagation of pore pressure from right to left within FGM zone

The visualization module's contour plots commonly indicate the average value for the output parameter over a certain element of the fault gouge material. The pore pressure graph in figure 4.15 at the selected node 3844 in the center of the materials represents the pore pressure against time.

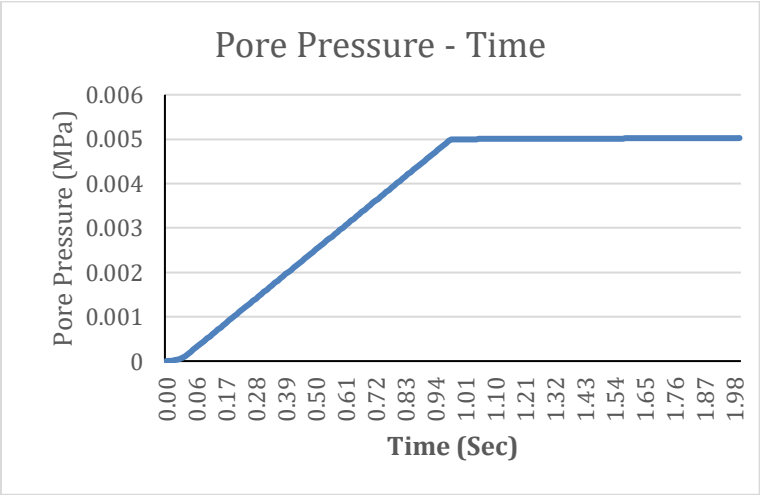

Figure 4-15: Pore pressure propagation with respect to time at central nodal 3844

The pore pressure after 1 second remains constant till the end. This is caused by the shear forces applied to the gouge materials during the horizontal movement of 5 cm in the second step from 1 to 2 seconds of time.

4.2.2 Total Fluid Volume Ratio (FLUVR)

Total Fluid Volume Ratio (FLUVR), which measures the fluid presence within the fault gouge material, affects the mechanical properties of the fault gouge materials.

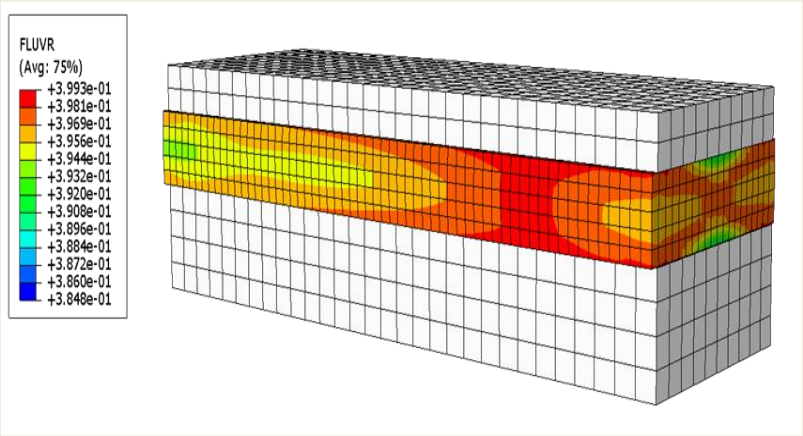

Figure 4-16: Total Fluid Volume Ratio (FLUVR), show the volume of fluid within the FGM zone

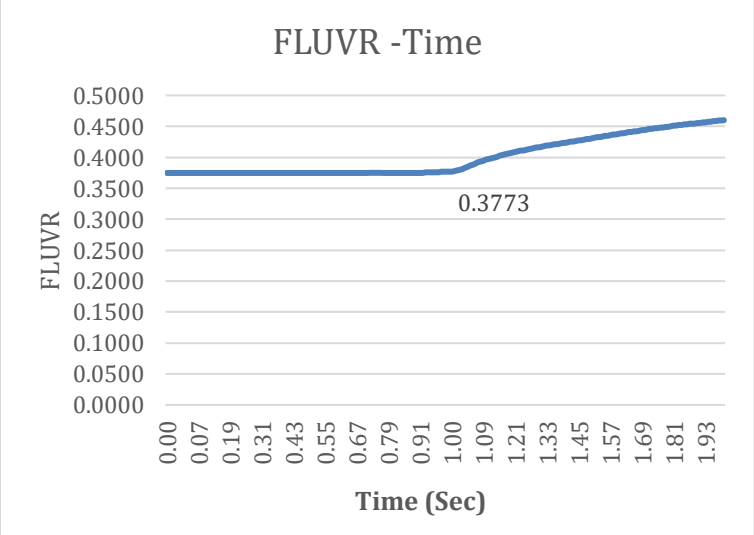

Figure 4-17: Total Fluid Volume Ratio (FLUVR) over time
at central FGM node3844

The above figure 4.17 shows a constant FLUVR around 0.3750, in the first step of 1 second, and subsequently increasing above the 1.5-second level. The observed increase in FLUVR indicates an increase in fluid volume at node 3844, potentially due to the shear movement of fault gouge material or the movement of fluid out of the node region, suggesting a rise in the volume of fluid at this particular node.

4.2.3 Stress Strain Analysis

The Mohr-Coulomb plasticity model provides a 3D representation of the fault gouge material under stress loading conditions, which is shown in figure 4.21. The below figure shows a visual distribution of the plastic strain magnitude for the fault gouge materials by applying a normal load of 1 MPa to the plastic model under the influence of the pore pressure. The color counter plot shows the magnitude of the plastic strain within the fault gouge material. The most intense is in the central right region of FGM, which suggests that this area is experiencing the most deformation, which is the focus area for our analysis to extract the data for stress strain analysis.

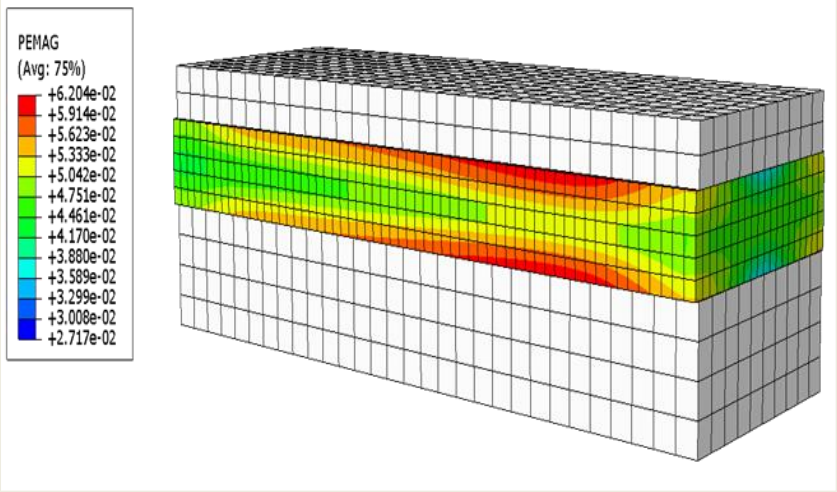

Figure 4-18: Plastic strain distribution under the influence of pore pressure

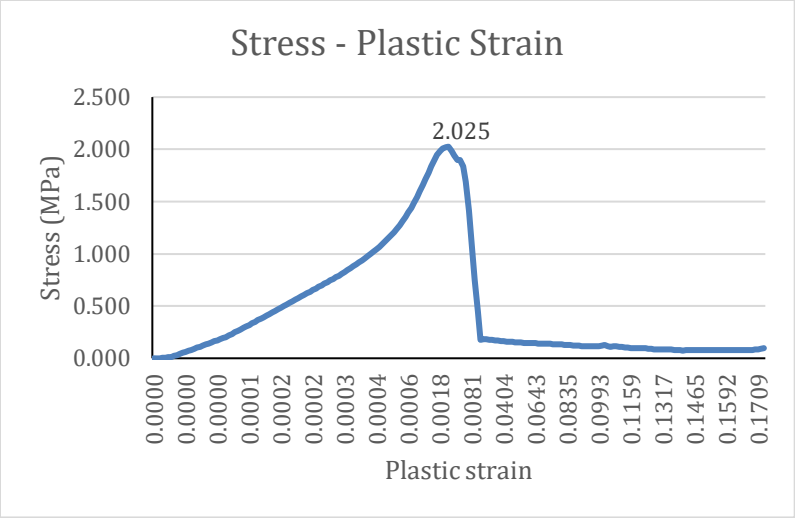

Figure 4-19: Stress-Strain relationship for FGM at specific node 3844

The above figure 4.19 shows the stress-plastic strain relationship for the FGM Mohr-Coulomb plasticity model at specific node 3844, which indicates the material response to the applied load. The maximum stress peak is about 2.02 MPa. The curve's drop after the peak stress shows the plastic mode of the FGM and the start of plastic deformation, which could be caused by strain hardening in the FGM material.

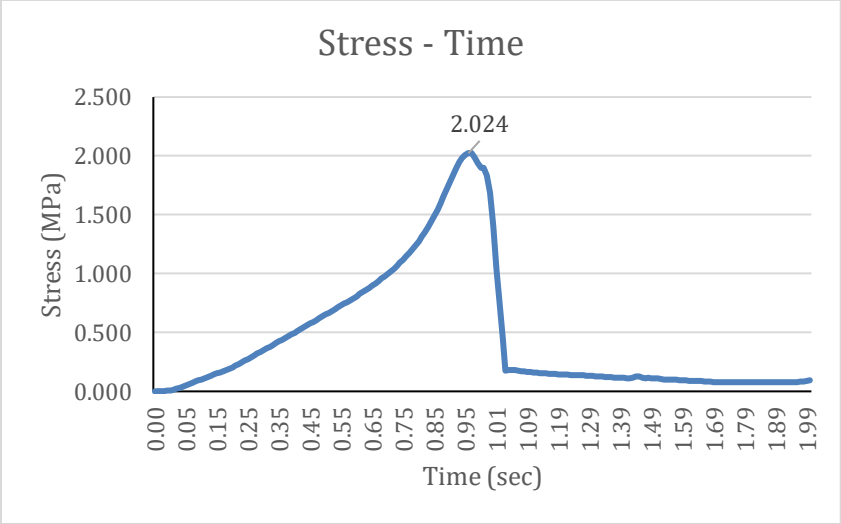

Figure 4-20: Stress-Time relationship for FGM at specific node 3844

The relationship between stress and time for a FGM at a specific location is denoted by the FGM node 3844. It illustrates how the stress level alters over an interval of 2 seconds at this particular

point in time, as shown in figure 4.20. At first, the stress level rises smoothly with the passage of time, reaching its highest peak point of 2.02 MPa in one second. Immediately after this peak load, the FGM goes under the plastic deformation and rapidly deceases in the second step, where the FGM is horizontally shear-moving 5 cm. This behavior indicates that the material reaches a yield point in the first normal load step and goes into plastic deformation after the shearing horizontally step time, as demonstrated by the fall in stress, which is shearing the FGM material in the second step of the model.

4.2.4 Total displacement

In the context of the normal load and shear load that have been applied in the model, the total displacement of the materials is depicted in figure 4.21, which can be seen below. This approach can be used in order to assess the total deformation of the FGM.

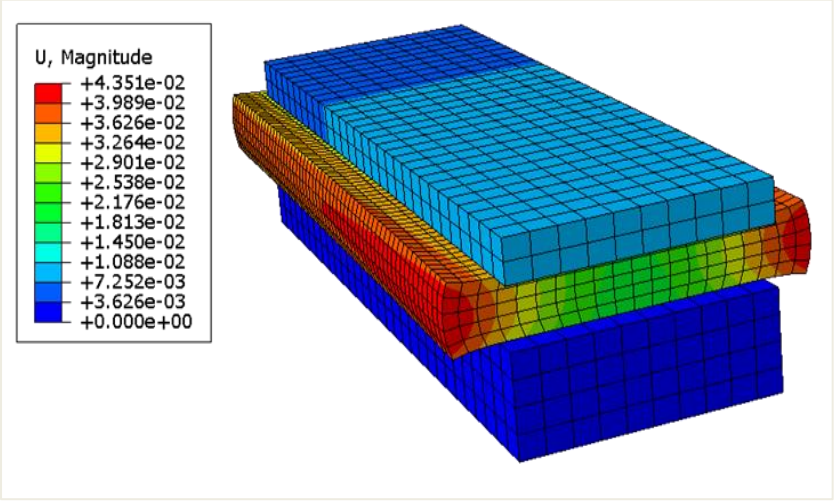

Figure 4-21: Total displacement of FGM in Mohr-Coulomb plasticity model

For the Mohr-Coulomb plasticity model for Fault Gouge Material (FGM), the maximum 1 MPa normal load is applied on the top steel plate and 2 cm horizontal movement of the FGM. The figure 4.21 show the total displacement magnitude and the FGM materials is expanded from the each side around 5 cm. However, figure 2.22 illustrates more specific look to the FGM material "U2"compaction between the steel plates where the contour plot show the value range from 0.006 cm to 0.6 cm.

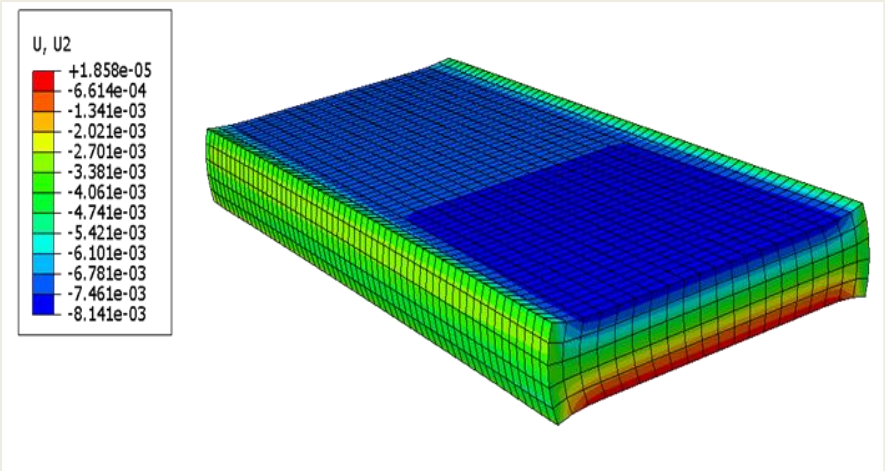

Figure 4-22: Total Displacement (U2) of the FGM in Mohr-Coulomb plasticity model

As a result of the computer's computing capabilities for the model, the model runs with a maximum normal load of 1 MPa and a horizontal movement of 2 cm.

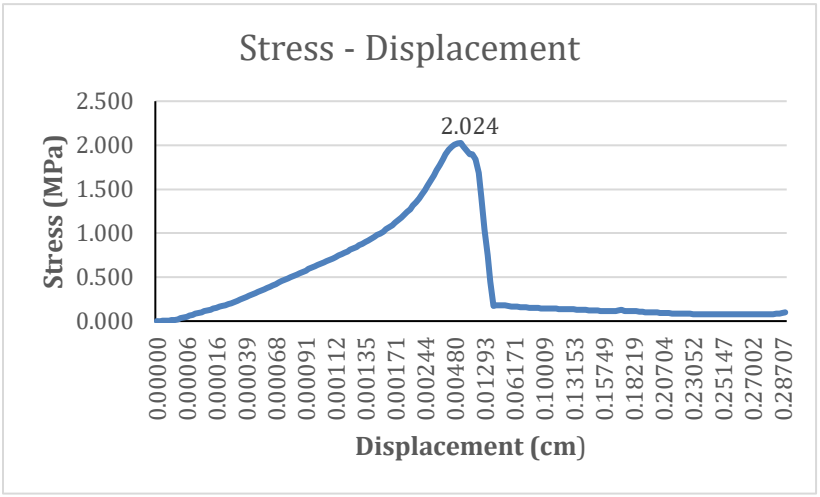

Figure 4-23: Stress-Displacement (U2) relation at specific node 3844 for FGM

Initially, the stress gradually increases with displacement in the first half of the line to reach the peak stress, which is approximately 2.024 MPa. At peak stress, the FGM goes under the plastic deformation, where it shows some fluctuation and decreases rapidly in the second shear step of the horizontal movement of the gouge materials. The graph shows an overall displacement of around 0.28 cm vertically at FGM node 3844.

4.3 Discussion of the Results

From the above section and explanation as well from the graphs of the pore pressure, fluid volume ratio, stress-strain analysis, and total displacement based on simulations that has been mentioned above. Both models of elasticity and Mohr Coulomb plasticity provide an understanding of the mechanical behavior of fault gouge material (FGM) under various loading conditions as shown in figure 4.24. To compare and analyze the Elasticity Model with the Mohr-Coulomb Plasticity Model, the use of the Elasticity Model is particularly suitable for cases where the material is supposed to primarily show elastic deformation, which shows a more simplified understanding of the FGM zone.

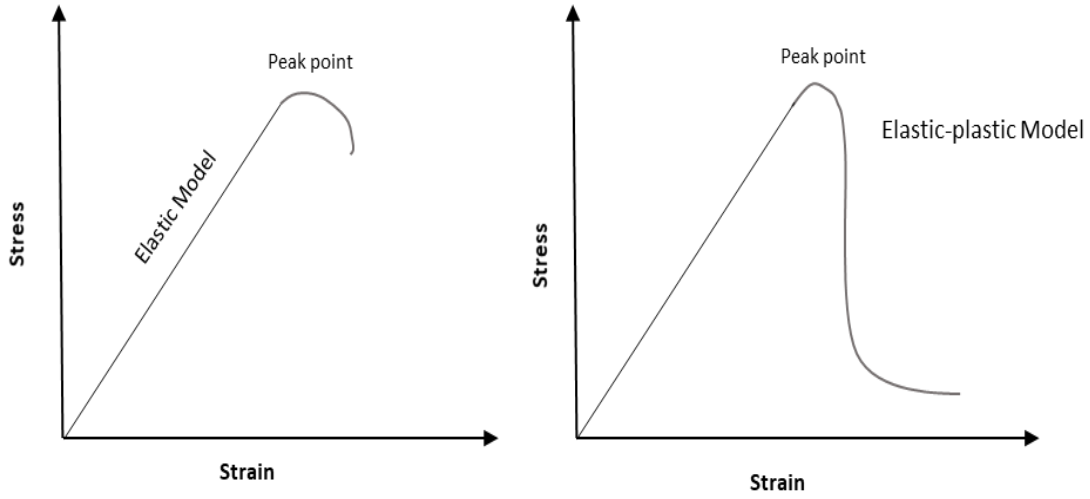

Figure 4-24 illustrate the Stress - Strain relation for elastic and Mohr coulomb plasticity model

The Mohr Coulomb plasticity model takes into account nonlinear behavior and yielding, which makes it better for modeling how the fault gouge material will behave closer to failure conditions. The fluid volume ratio fluctuation shows that fluid movement, material compaction, and shear forces all work together in a complicated way in the fault gouge material. This behavior shows how fault-gouge materials change when they are under stress and how fluids can change their mechanical properties.

4.4 Comparative analysis of the results

In this section, a comparative analysis of four models, specifically to examine two elastic models and two plastic models, both with and without pore pressure. These models will be further elaborated upon in separate steps, Step 1 (normal load) and Step 2 (shear load).

4.4.1 Elastic Model Analysis

I. Elastic strain

The provided figures illustrate a graphical representation of the elastic stress-strain experienced by the fault gouge materials when subjected to a normal load of 4 MPa inside the elastic model, while considering the impact of pore pressure and without pore pressure.

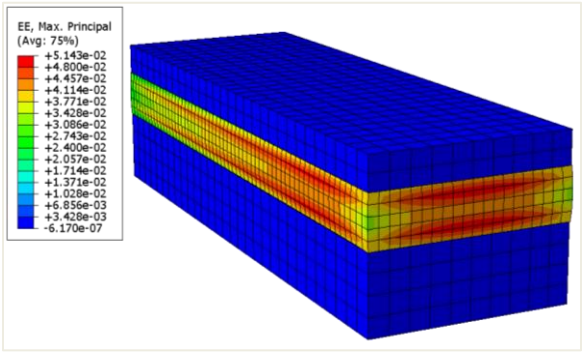

a. EE- Model-1 with pore pressure Step 1

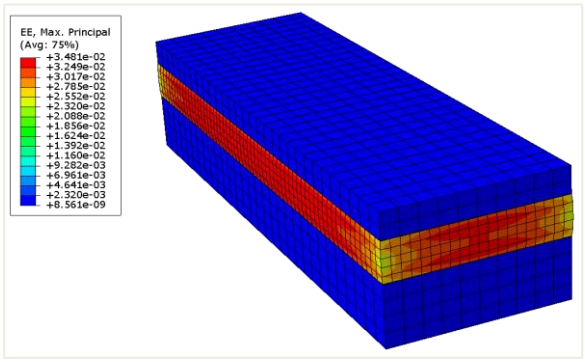

b. EE- Model-2 without pore pressure Step 1

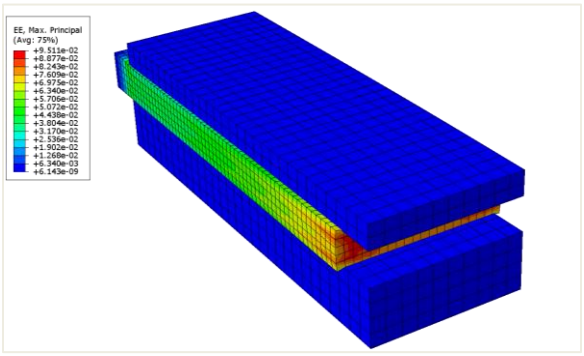

c. EE- Model-1 with pore pressure Step 2

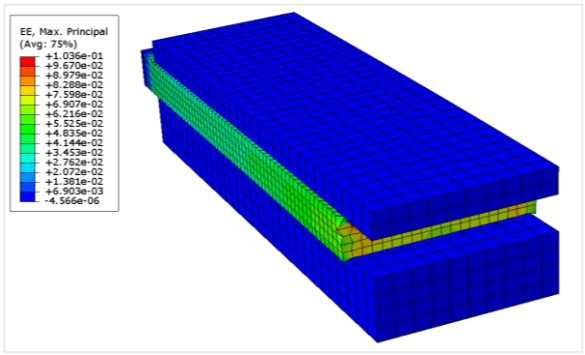

d. EE- Model-2 without pore pressure Step 2

Figure 4-25: (a) EE, Max principal under the influence of Pore Pressure (PP) in normal loading condition (b) EE, Max Principle without PP in normal loading condition (c) and (d) Shown FGM shear horizontally 5 cm with and without PP condition respectively

As it is shown in Figure 4.25 in Step 1 of the model by applying a 4 MPa normal load in the elastic model, in Section (a), the contour plot shows the more intense elastic strain (EE) magnitude around 0.04–0.03 in the center right of the FGM from where the pore pressure (PP) was applied, which suggests that this area is experiencing the most deformation, while in the case of Model 2, the intensity of the Max EE is the same over all regions of the FGM. Overall, the EE max principal in the elastic model-1 with pore pressure has more deformation EE in comparison to the EE model-2 without pore pressure in the first step of the model.

Moreover, in step 2 of models (c) and (d), where the FGM were sheared to move horizontally 5 cm from left to right, the EE max principal strain showed quite similar values in the contour plots; however, the Model-2 without pore pressure showed some distortions of the elements. The observed element distortion at a horizontal distance of 5 cm represents the maximum displacement that the FGM material can move horizontally based on the specified input properties.

II. Displacement U2 Compression of FGM zone

The fault gouge material (FGM) is compressed between two steel plates, resulting in compressing along the y-axis in the U2 direction. The displacement of the FGM in the y-axis direction is shown in Figure 4.26 for Steps 1 and 2 of the EE models, both with and without pore pressure. Negative values are observed in contour plots due to an opposite direction going in a downward direction.

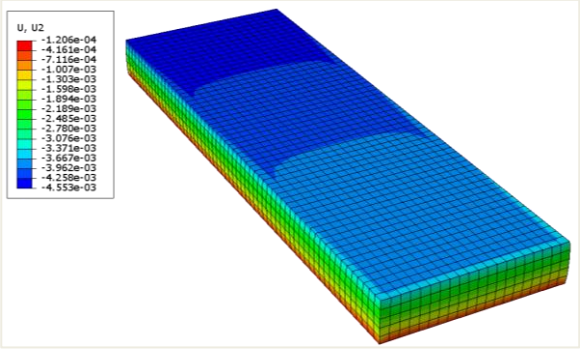

a. U2-displacement- with Pore Pressure Step 1

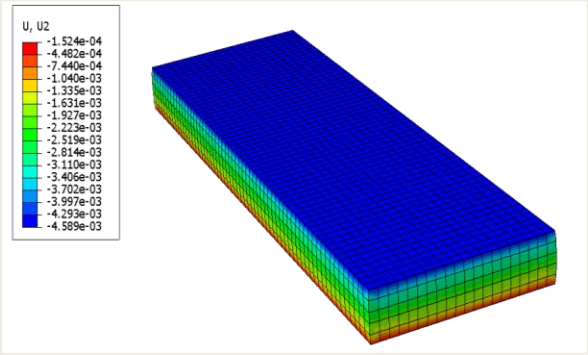

b. U2-displacement- without Pore Pressure Step 1

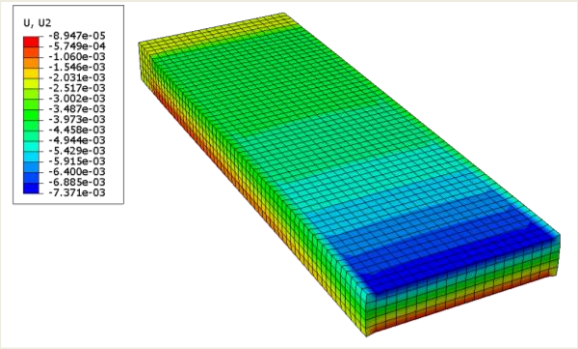

c. U2-displacement- with Pore Pressure Step 2

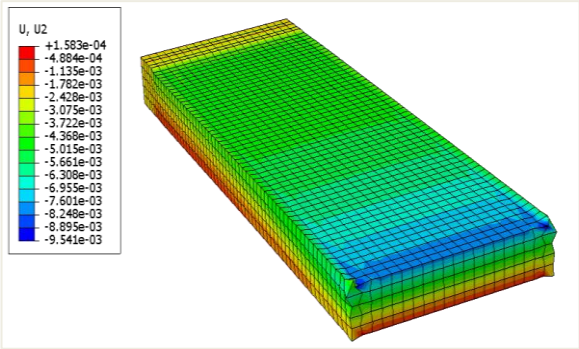

d. U2-displacement- without Pore Pressure Step 2

Figure 4 9: (a) U2, Y-axis deformation under the influence of PP in normal loading condition (b) U2, Y-axis without PP in normal loading condition (c) and (d) show FGM shear horizontally 5 cm with and without PP condition respectively

In step 1 of model 1, the addition of pore pressure (PP) results in small deformation compared to step 1 of model 2 without PP. This is particularly evident in the region where PP propagates from the right side x-axis, as shown in the contour plot within the range of 0.33 to 0.39 cm. On the other hand, model-2, which does not exhibit pore pressure, exhibits a relatively large deformation within the range of 0.39 to 0.45 cm on the outermost layer of the FGM.

After the horizontal shear movement of the FGM by 5 cm in step-2, the FGM in model-2 without PP exhibits a slightly higher overall deformation U2 within the range of 0.30 to 0.6 cm compared to model-1 with PP. However, the high pore pressure region of the FGM experiences smaller deformations compared to other regions.

4.4.2 Mohr-Coulomb plasticity model

I- MC-Plastic strain

As it is shown in Figure 4.27 in Step 1 of the Mohr Coulomb Plasticity models (MC-Model 1 and 2), by applying a 1 MPa normal load, the MC model-1 (a) shows the plastic strain magnitude in the range of 0.008–0.016, but a slightly higher show in the spot of the FGM from where the pore pressure (PP) was applied, which is suggesting that this area is experiencing the maximum plastic deformation (PE), while in the case of model-2 the intensity of the PE is the same over all regions of the FGM zone.

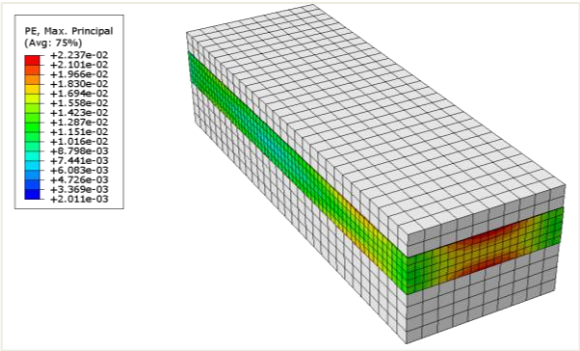

a. MC Plasticity Model-1 with Pore Pressure Step 1

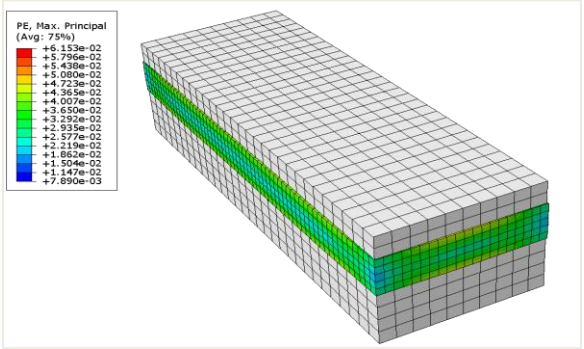

b. MC Plasticity Model-2 without Pore Pressure Step 1

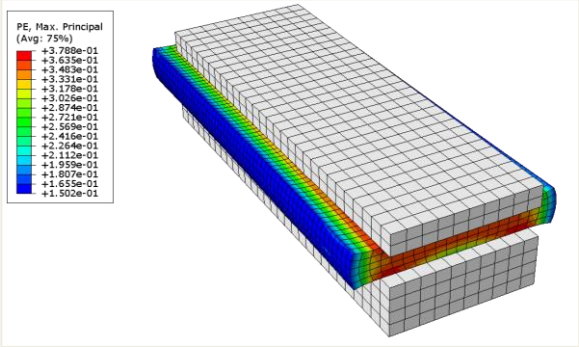

c. MC Plasticity Model-1 with Pore Pressure Step 2

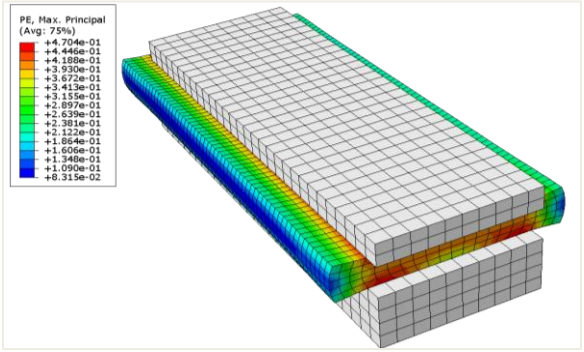

d. MC Plasticity Model-2 without Pore Pressure Step 2

Figure 4-27: (a) PE, Max principal under the influence of Pore pressure (PP) in normal loading condition (b) PE, Max Principle without PP in normal loading condition (c) and (d) Shown FGM shear horizontally 2 cm with and without PP condition respectively

Overall, the PE max principal in step 1 with pore pressure has a slightly smaller PE max compared to the MC-Model-2 without pore pressure in the first step of the model. .

Furthermore, in the 2nd step of models (c) and (d), the FGM zone was subjected to a horizontal shear movement of 2 cm from left to right in the opposite direction of the x-axis. The MC-Model-2 without PP exhibited a higher maximum principal strain (PE max) compared to the MC-Model-1 with Pore pressure (PP).

II- MC-U2-displacement (Compression of the gouge material in Y-direction)

The results from the contour plots in Figure 4.28 shows the compression of the FGM zone in MC-Models, showing the U2 deformation on the y-axis and negative values in the contour plots due to the opposite downward orientation.

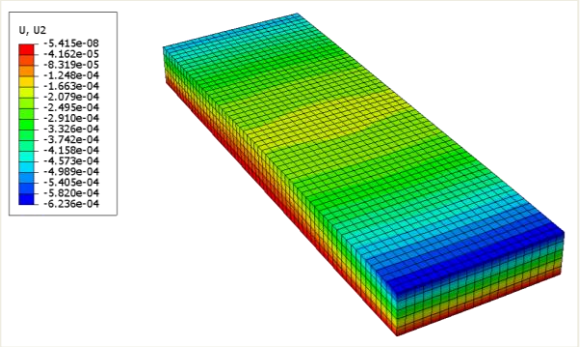

b. MC Plasticity Model-1 with Pore Pressure Step 1

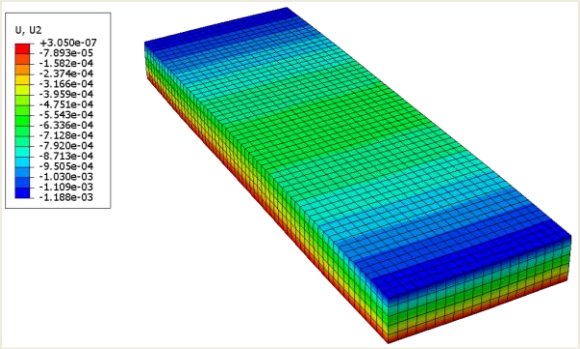

a. MC Plasticity Model-2 without Pore Pressure Step 1

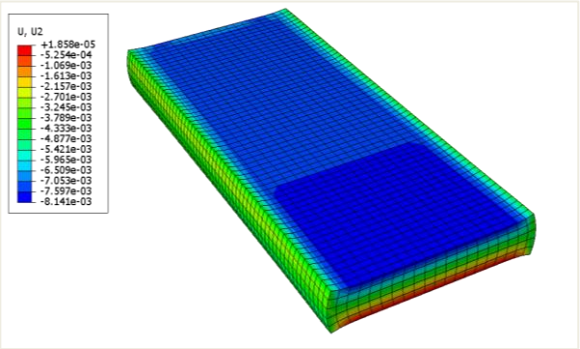

d. MC Plasticity Model-1 with Pore Pressure Step 2

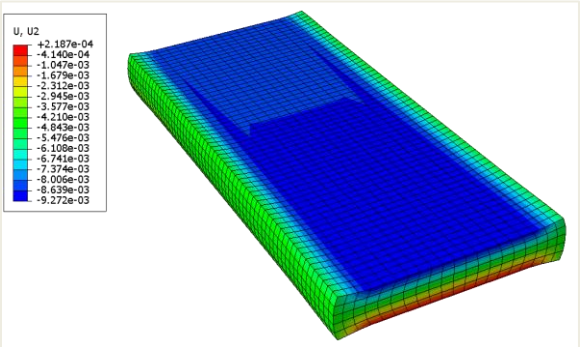

c. MC Plasticity Model-2 without Pore Pressure Step 2

Figure 4-10: (a) U2, Y-axis deformation under the influence of PP in normal loading condition (b) U2, Y-axis without PP in normal loading condition (c) and (d) show FGM shear horizontally 2 cm with and without PP condition respectively

After step 1, the FGM zone shows minor deformation in both models. However, the MC-Model-2 without PP demonstrates significant deformation ranging from 0.004 to 0.01 cm, in contrast to the MC-Model-1 with PP. After horizontally moving the FGM in step 2, the contour plots indicate that the U2 values are slightly higher for MC-Model-2 without PP compared to MC-Model-1 with PP.

Furthermore, the Mohr Coulomb plasticity model exhibits excessive bulking of the FGM when subjected to a shear of 2 cm, resulting in an estimated displacement of 4.4 cm on each side, as

shown in Figure 4.29. Which attention to the significant effect of shear load on the deformation behavior of FGM in the given boundary and loading condition conditions.

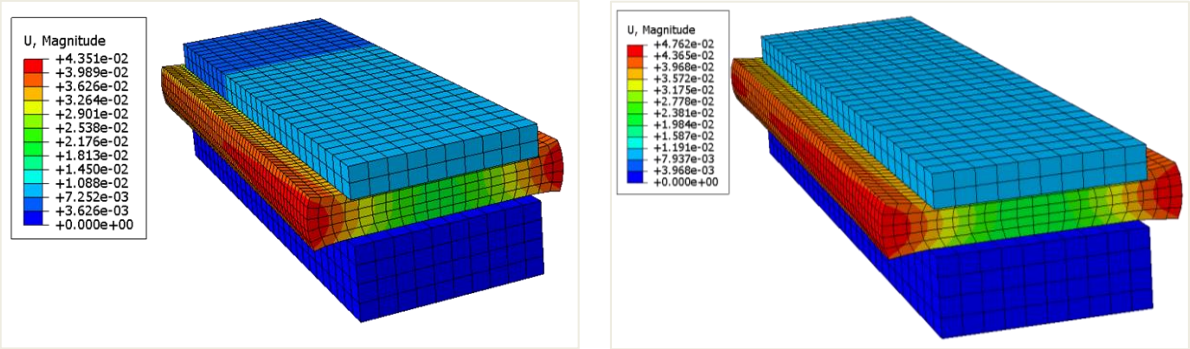

Figure 4-29: (Left) Total deformation in MC-Model-1 Step 2 under the influence of Pore pressure (right) total displacement (U) MC-Model-2-Step-2 FGM shear horizontally 2 cm without PP

5. Conclusions and limitation

The two models elastic and plastic model were created for the fault gouge materials (FMG) zone between two steel plates to investigate the mechanical behavior of the material in Abaqus Software. All over the results, contour plots and graphs show quite satisfactory results for the FGM zone. Using the technique of simulations in FEM, we were able to get a comprehensive understanding of the mechanical behavior of selected fault-gouge materials under normal and shear loading conditions. The elasticity model and the Mohr-Coulomb plasticity model demonstrated the material's response to axial normal and shear loading, as well as the effects of pore pressure on the material's deformation and shear response. The comparison of the results reveals that the existence of pore pressure has an evident effect on the deformation characteristics of the FGM. Moreover, to illustrate the dynamic changes that occur within the material when it is subjected to stress, an analysis of the pore pressure and total fluid volume ratio (FLUVR) throughout the course of time at a particular node was carried out. With regard to the elasticity model, it has been found that pore pressure propagation has a major influence on the deformation rate and shear response of the fault-gouge materials. To conclude, our research study shows notable progress in the numerical simulation of fault gouge materials, offering unique perspectives on their mechanical response to pore pressures and stresses. These results have the potential to enhance the understanding of the mechanical behavior of the fault-gouge materials.

Based on our findings from the simulations, many recommendations are needed to enhance the investigation of fault-gouge materials. Future studies should consider refining the models to include more complex geological features, such as joints, fractures etc. for a more realistic simulation of subsurface conditions, which would require more computational power to run.
The understanding of fault mechanics and the scale-dependent nature of fault gouge (FGM) behavior could be improved through the utilization of a multi-scale approach that takes into account both the micro-level and the macro-level behaviors of FGM by using more computational power with pair programming, for instance, fluidity with FEM analysis. Moreover, the long-term behavior of FGM under loading and pore pressure conditions could increase the understanding of the long term behavior of faults.

Our study does have some limitations, which have more major consequences for the accuracy and applicability of the findings. These limitations are presented in the following sentence.

The current numerical models do not consider the influence of carbon dioxide (CO2) on the fault gouge materials (FGMs). This is a significant drawback, as carbon dioxide has the potential to impact the mechanical characteristics of FGMs, especially when considering the storage conditions relevant to Carbon Capture and Storage (CCS) applications. Future models should consider the physical and chemical interactions between CO2 and FGM to gain a comprehensive understanding of their impact on fault stability and integrity in CCS contexts.

Another limitation arises from the extrusion of FGM from the shear box during simulations. This observation implies that the model does not accurately simulate the physical limitations found at actual fault zones. The extrusion indicates that there may be some problems with the boundary conditions or mechanical setup of the model, which could result in an error of the confinement pressures and shear strength of the FGM. This limitation is quite significant as it has the potential to cause gaps between the predicted and actual responses of fault zones under stress. As a result, the reliability of the model for predictive analyses may be limited. Future iterations of the model should focus on addressing these issues to better align the setup with real-world conditions, thereby improving the accuracy of the simulation results.

6. References

1. Bachu, S. (2015). "Review of CO2 storage efficiency in deep saline aquifers." International Journal of Greenhouse Gas Control **40**: 188-202.
2. Barbero, E. J. (2023). Finite element analysis of composite materials using Abaqus®, CRC press.
3. Ben-Zion, Y. and C. G. Sammis (2003). "Characterization of fault zones." Pure and applied geophysics **160**: 677-715.
4. Bense, V., T. Gleeson, S. Loveless, O. Bour and J. Scibek (2013). "Fault zone hydrogeology." Earth-Science Reviews **127**: 171-192.
5. Brekke, T. L. and T. R. Howard (1973). Functional classification of gouge materials from seams and faults in relation to stability problems in underground openings, University of California, Department, of Civil Engineering.
6. Byerlee, J. (1990). "Friction, overpressure and fault normal compression." Geophysical Research Letters **17**(12): 2109-2112.
7. Crawford, B., D. Faulkner and E. Rutter (2008). "Strength, porosity, and permeability development during hydrostatic and shear loading of synthetic quartz-clay fault gouge." Journal of Geophysical Research: Solid Earth **113**(B3).
8. Delle Piane, C., A. Giwelli, M. B. Clennell, L. Esteban, M. C. D. N. Kiewiet, L. Kiewiet, S. Kager and J. Raimon (2016). "Frictional and hydraulic behaviour of carbonate fault gouge during fault reactivation—An experimental study." Tectonophysics **690**: 21-34.
9. Faulkner, D., T. Mitchell, D. Healy and M. Heap (2006). "Slip on'weak'faults by the rotation of regional stress in the fracture damage zone." Nature **444**(7121): 922-925.
10. Faulkner, D. and E. Rutter (2000). "Comparisons of water and argon permeability in natural clay-bearing fault gouge under high pressure at 20° C." Journal of Geophysical Research: Solid Earth **105**(B7): 16415-16426.
11. Faulkner, D. R., C. Sanchez-Roa, C. Boulton and S. Den Hartog (2018). "Pore fluid pressure development in compacting fault gouge in theory, experiments, and nature." Journal of Geophysical Research: Solid Earth **123**(1): 226-241.

12. Fei, K. (2016). "Experimental study of the mechanical behavior of clay–aggregate mixtures." Engineering geology **210**: 1-9.
13. Giwelli, A., C. Delle Piane, L. Esteban, M. Clennell, J. Dautriat, J. Raimon, S. Kager and L. Kiewiet (2016). "Laboratory observations of fault transmissibility alteration in carbonate rock during direct shearing." Geofluids **16**(4): 658-672.
14. Haines, S. H., B. Kaproth, C. Marone, D. Saffer and B. Van der Pluijm (2013). "Shear zones in clay-rich fault gouge: A laboratory study of fabric development and evolution." Journal of Structural Geology **51**: 206-225.
15. Hirakawa, E. and S. Ma (2016). "Dynamic fault weakening and strengthening by gouge compaction and dilatancy in a fluid-saturated fault zone." Journal of Geophysical Research: Solid Earth **121**(8): 5988-6008.
16. Hubbert, M. K. (1959). "Role of fluid pressure in mechanics of over-thrust faulting." Geol. Soc. Am. Bull. **48**: 1459-1519.
17. Ikari, M. J., D. M. Saffer and C. Marone (2009). "Frictional and hydrologic properties of clay-rich fault gouge." Journal of Geophysical Research: Solid Earth **114**(B5).
18. Makhnenko, R. Y., V. Vilarrasa, D. Mylnikov and L. Laloui (2017). "Hydromechanical aspects of CO2 breakthrough into clay-rich caprock." Energy Procedia **114**: 3219-3228.
19. Marone, C., C. B. Raleigh and C. Scholz (1990). "Frictional behavior and constitutive modeling of simulated fault gouge." Journal of Geophysical Research: Solid Earth **95**(B5): 7007-7025.
20. Morrow, C. A., L. Q. Shi and J. Byerlee (1984). "Permeability of fault gouge under confining pressure and shear stress." Journal of Geophysical Research: Solid Earth **89**(B5): 3193-3200.
21. Phillips, T., N. Kampman, K. Bisdom, N. D. F. Inskip, S. A. den Hartog, V. Cnudde and A. Busch (2020). "Controls on the intrinsic flow properties of mudrock fractures: A review of their importance in subsurface storage." Earth-Science Reviews **211**: 103390.
22. Pichler, T., T. Pucker, T. Hamann, S. Henke and G. Qiu (2012). High-Performance Abaqus Simulations in Soil Me-chanics Reloaded–Chances and Frontiers. 2012 SIMULIA Community Conference.
23. Rao, S. S. (2017). The finite element method in engineering, Butterworth-heinemann.

24. Rawling, G. C., L. B. Goodwin and J. L. Wilson (2001). "Internal architecture, permeability structure, and hydrologic significance of contrasting fault-zone types." Geology **29**(1): 43-46.
25. Reches, Z. e. and T. A. Dewers (2005). "Gouge formation by dynamic pulverization during earthquake rupture." Earth and Planetary Science Letters **235**(1-2): 361-374.
26. Rojstaczer, S., S. Wolf and R. Michel (1995). "Permeability enhancement in the shallow crust as a cause of earthquake-induced hydrological changes." Nature **373**(6511): 237-239.
27. Sammis, C. G., R. H. Osborne, J. L. Anderson, M. Banerdt and P. White (1986). "Self-similar cataclasis in the formation of fault gouge." Pure and Applied Geophysics **124**: 53-78.
28. Scuderi, M. M. and C. Collettini (2016). "The role of fluid pressure in induced vs. triggered seismicity: Insights from rock deformation experiments on carbonates." Scientific reports **6**(1): 24852.
29. Sibson, R. H. (2000). "Fluid involvement in normal faulting." Journal of Geodynamics **29**(3-5): 469-499.
30. Tao, M., Q. Ren, H. Bian, M. Cao and Y. Jia (2022). "Mechanical Properties of Soil-Rock Mixture Filling in Fault Zone Based on Mesostructure." CMES-Computer Modeling in Engineering & Sciences **132**(2).
31. Terzaghi, K. (1943). Theoretical soil mechanics.
32. Treffeisen, T. and A. Henk (2020). "Elastic and Frictional Properties of Fault Zones in Reservoir-Scale Hydro-Mechanical Models—A Sensitivity Study." Energies **13**(18): 4606.
33. Twiss, R. J. and E. M. Moores (1992). Structural geology, Macmillan.
34. Update, P. (2011). "SIMULIA."
35. Vannucchi, P., A. Maltman, G. Bettelli and B. Clennell (2003). "On the nature of scaly fabric and scaly clay." Journal of Structural Geology **25**(5): 673-688.
36. Wei, H., W. Xu, C. Wei and Q. Meng (2018). "Influence of water content and shear rate on the mechanical behavior of soil-rock mixtures." Science China Technological Sciences **61**: 1127-1136.

37. Zhang, Z.-L., W.-J. Xu, W. Xia and H.-Y. Zhang (2016). "Large-scale in-situ test for mechanical characterization of soil–rock mixture used in an embankment dam." International Journal of Rock Mechanics and Mining Sciences **86**: 317-322.
38. Zheng, X. and D. N. Espinoza (2021). "Multiphase CO2-brine transport properties of synthetic fault gouge." Marine and Petroleum Geology **129**: 105054.